Since January 2020 Elsevier has created a COVID-19 resource centre with free information in English and Mandarin on the novel coronavirus COVID-19. The COVID-19 resource centre is hosted on Elsevier Connect, the company's public news and information website.

Biosensors and Bioelectronics 219 (2023) 114783

Contents lists available at ScienceDirect

Biosensors and Bioelectronics

journal homepage: www.elsevier.com/locate/bios

Microfluidic nanodevices for drug sensing and screening applications

Arnab Pal [a,b,1], Kuldeep Kaswan [a,b,1], Snigdha Roy Barman [a,b], Yu-Zih Lin [a], Jun-Hsuan Chung [c], Manish Kumar Sharma [d], Kuei-Lin Liu [a], Bo-Huan Chen [a,b,g], Chih-Cheng Wu [a,h,i,j], Sangmin Lee [k,***], Dongwhi Choi [l,**], Zong-Hong Lin [a,b,c,e,f,l,*]

[a] Institute of Biomedical Engineering, National Tsing Hua University, Hsinchu, 30013, Taiwan
[b] International Intercollegiate PhD Program, National Tsing Hua University, Hsinchu, 30013, Taiwan
[c] Department of Power Mechanical Engineering, National Tsing Hua University, Hsinchu, 30013, Taiwan
[d] Department of Materials Science and Engineering, National Tsing Hua University, Hsinchu, 30013, Taiwan
[e] Department of Chemistry, National Tsing Hua University, Hsinchu, 30013, Taiwan
[f] Frontier Research Center on Fundamental and Applied Sciences of Matters, National Tsing Hua University, Hsinchu, 30013, Taiwan
[g] Department of Gastroenterology and Hepatology, Chang Gung Memorial Hospital, Linkou Medical Center, Taoyuan, 333, Taiwan
[h] Center of Quality Management, National Taiwan University Hospital, Hsinchu Branch, Hsinchu, 30059, Taiwan
[i] College of Medicine, National Taiwan University, Taipei, 10051, Taiwan
[j] Institute of Cellular and System Medicine, National Health Research Institute, Zhunan, 35053, Taiwan
[k] School of Mechanical Engineering, Chung-Ang University, Seoul, 06974, South Korea
[l] Department of Mechanical Engineering (Integrated Engineering Program), Kyung Hee University, Gyeonggi, 17104, South Korea

ARTICLE INFO

Keywords:
Microfluidics
Nanosensors
Illicit drugs
Sensing techniques
Nanomaterials

ABSTRACT

The outbreak of pandemics (e.g., severe acute respiratory syndrome coronavirus 2 (SARS-CoV-2 in 2019), influenza A viruses (H1N1 in 2009), etc.), and worldwide spike in the aging population have created unprecedented urgency for developing new drugs to improve disease treatment. As a result, extensive efforts have been made to design novel techniques for efficient drug monitoring and screening, which form the backbone of drug development. Compared to traditional techniques, microfluidics-based platforms have emerged as promising alternatives for high-throughput drug screening due to their inherent miniaturization characteristics, low sample consumption, integration, and compatibility with diverse analytical strategies. Moreover, the microfluidic-based models utilizing human cells to produce in-vitro biomimetics of the human body pave new ways to predict more accurate drug effects in humans. This review provides a comprehensive summary of different microfluidics-based drug sensing and screening strategies and briefly discusses their advantages. Most importantly, an in-depth outlook of the commonly used detection techniques integrated with microfluidic chips for highly sensitive drug screening is provided. Then, the influence of critical parameters such as sensing materials and microfluidic platform geometries on screening performance is summarized. This review also outlines the recent applications of microfluidic approaches for screening therapeutic and illicit drugs. Moreover, the current challenges and the future perspective of this research field is elaborately highlighted, which we believe will contribute immensely towards significant achievements in all aspects of drug development.

1. Introduction

Due to the emergence of pandemics (e.g., SARS-CoV-2, H1N1), epidemics (e.g., Ebola virus disease (EVD in 2014), Zika virus (ZIKV in 2016), etc.) (Carroll et al., 2021; Telenti et al., 2021; Wang and Wu, 2018; Yakob et al., 2022), and rapid growth of new diseases, the demand for novel drugs screening have become a topic of high interest. The recent paradigm of pharmaceutical invention has rendered drug development a prolonged and increasingly expensive process. Several studies have reported that it takes more than ten years, on average, to develop

* Corresponding author. Institute of Biomedical Engineering, National Tsing Hua University, Hsinchu, 30013, Taiwan.
** Corresponding author.
*** Corresponding author.
E-mail addresses: slee98@cau.ac.kr (S. Lee), dongwhi.choi@khu.ac.kr (D. Choi), linzh@mx.nthu.edu.tw (Z.-H. Lin).
[1] These authors contributed equally to this work.

https://doi.org/10.1016/j.bios.2022.114783
Received 19 June 2022; Received in revised form 18 September 2022; Accepted 1 October 2022
Available online 5 October 2022

and bring a safe and effective new drug to the market. The average expenditure for a new medicine to reach the market has doubled every decade for the last 40 years (Wang et al., 2018a). Due to this increase in financial burden, most of the identified initial compounds with potential health advantages are steadily eliminated during the clinical-stage periods (Harrer et al., 2019a). Furthermore, approximately 20 million animal subjects (mouse and rat models) are employed as in vivo models to test new pharmaceutical compounds prior to human trials (Driouich et al., 2021). In addition, the use of animals in research has been recently brought into question by the scientific community due to concerns regarding clinical validity, applicability, and ethics (Robinson et al., 2019). Hence, there is an urgent need to develop new techniques for drug screening with improved predictability and clinical outcomes and can achieve the goal of sustainable drug development.

In this regard, microfluidic technology has emerged as a promising platform for miniaturized and controlled drug screening, even at the cellular level (Ramezankhani et al., 2022). Compared to single-drug analysis in conventional petri dish or animal model methods, microfluidic platforms can simultaneously provide high-precision multidrug (Jiang et al., 2003; Mitxelena-Iribarren et al., 2019; Zhao et al., 2021) and multiconcentration (Humphries et al., 2018; Bavli et al., 2016; Lee et al., 2019b; Liu et al., 2019) screening with high sensitivity and faster response times. The inherent potential to design microfluidic devices with dimensions compatible with single cells has attracted considerable attention for studying the biochemical functions of cells, which is necessary for new drug development. Moreover, microfluidic systems can act as an ideal platform for precise control of the concentration gradients of drugs to analyze the cellular phenotypes that react to chemical and physical stimuli in the extracellular microenvironment, thus allowing real-time monitoring (Berthier and Beebe, 2014; Hu et al., 2018). In the 1990s, microfluidics-based devices were first introduced to enable cell culture and drug analysis in different cell lines for pharmaceutical screening. Since then, the field has undergone massive transformation, such as dramatically reducing the sample volume to single droplets and extending the platform for the screening a wide variety of drug targets. In addition, microfluidic systems have high potential to revolutionize drug screening (Valencia et al., 2012), from nanoparticle synthesis to clinical trials (Feng et al., 2017) and from single droplet (Chowdhury et al., 2019; Eduati et al., 2018; Gérard et al., 2020; Sabhachandani et al., 2016) to multiorgan system analysis (Jin et al., 2018; Zheng et al., 2021). Furthermore, human organs can be mimicked in microfluidic systems to simulate a typical human organ's microstructure and physiological operations (Skardal et al., 2016; Zheng et al., 2016). Currently, lung (Jung et al., 2019; Xu et al., 2013; Zhu et al., 2022), liver (Delalat et al., 2018; Lee et al., 2019a), heart (Liu et al., 2020; Ren et al., 2020; F. Zhang et al., 2021), kidney (Lin et al., 2020; Theobald et al., 2018), blood vessels (Cao et al., 2019; Lee et al., 2021) and even the whole body (Chen et al., 2018) can be mimicked on microfluidic devices, which results in more predictable outcomes for drug screening. These outstanding characteristics make microfluidic systems an ideal choice for highly sensitive drug sensing and screening. (Mullard, 2018).

To date, the developments and advancements in microfluidics-based drug sensing and screening have been reviewed by several research groups (Wang et al., 2018; Harrer et al., 2019; Dhiman et al., 2019; Harrer et al., 2019b; Liu et al., 2019; Liu et al., 2021; Musile et al., 2021; Ramezankhani et al., 2022; Wang et al., 2018b; Zhai et al., 2019; Zhao et al., 2020). Wang et al. explored multiorgan integrated platforms with total tissue and fluid volumes less than 1/10000 of that of the human body (≈6.5 mL) that were capable of drug testing and disease modeling (Wang et al., 2018). Moreover, Harrer et al. specifically reviewed how current advances in artificial intelligence (AI) can reshape critical stages of clinical trial strategies to improve their success rates (Harrer et al., 2019). Furthermore, cell-based microfluidic technologies for drug screening were reviewed and discussed by Zhai and coworkers (Zhai et al., 2019). In addition, few of the reported studies were specifically dedicated to anticancer drug screening and its influence on cancer therapy. For instance, Dhiman et al. primarily reviewed the current challenges in microfluidics-based chemotherapy, such as combinatorial drug therapy, drug resistance, cancer metastasis, and personalized medicine. (Dhiman et al., 2019). In another review, Shi et al. focused on current advancements in microfluidic devices for anticancer drug screening and inventions in tumor tissue chips with emphasis on the choice of materials (especially hydrogels) in designing a microfluidic platform to simulate a dedicated tumor microenvironment (Shi et al., 2021). Furthermore, Zhao and coworkers presented a summary of the rational design and fabrication of microfluidic devices based on biomedical materials (Zhao et al., 2020). In addition to anticancer drugs some groups have emphasized recent advances in screening for other drug types, such as illegal drugs. Musile et al. provided a short synopsis of the fabrication and detection methods for designing paper-based microfluidic devices for the forensic analysis of illegal drugs (Musile et al., 2021). Subsequently, Liu et al. presented an overall assessment of the revolutionary influences of microfluidics on the whole drug development system, i.e., drug synthesis, drug screening, drug delivery, and drug evaluation (Liu et al., 2021). In a recent review, Ramezankhani and coworkers discussed the potential of microfluidics-based systems for studies of SARS CoV-2 and the screening of potential therapeutic drugs for coronavirus 2019 (COVID-19) (Ramezankhani et al., 2022).

Nevertheless, most of the existing literature did not provide an extensive and in-depth survey of the overall developments in microfluidics-based drug sensing and screening. In this review, for the first time, we have highlighted the importance of the detection methods, sensing and fabrication materials and properties of microfluidic channels that significantly influence drug screening performance at the microscale. The first section includes a comprehensive overview of the detection techniques, particularly optical, electrochemical, and mass-spectroscopic-based modalities, which are widely used for microfluidic drug sensing and screening. Then, valuable information on the influence of the sensing surface materials, fabrication materials, surface morphology, and the advantages of different geometrical designs of the microfluidic prototypes are also highlighted. This section is intended to provide a critical understanding of the structural properties of the microchannels and their impact on drug screening sensitivity. Then, applications of microfluidic systems for therapeutic and illicit drugs are discussed. Lastly, existing challenges, and future prespectives in drug screening and sensing applications of microfluidics technology have also been underlined. We believe that this review will enhance readers understanding of the recent innovations in the field of microfluidics-based drug sensing and facilitate new advances toward developing more precise drug screening methodologies. Fig. 1 summarizes different microfluidics-assisted drug sensing and screening techniques; the influence of sensing materials, surface morphology, and geometrical designs of the platforms; and their respective applications in therapeutic and illicit drug screening.

2. Techniques

2.1. Optical techniques

Optical sensors have emerged as an innovative and compelling tool that has been widely employed in screening drugs for various biomedical, environmental monitoring, food safety, and forensic analysis applications (Mao et al., 2020; Mitchell et al., 2022; Musile et al., 2021). Generally, an optical probe is functionalized onto the microfluidic channel, which possesses a specific binding affinity to the drug molecules, resulting in the generation of a signal that varies with the concentration of the drug immobilized. Depending on the type of detection, optical sensors are primarily classified into fluorescence-based, surface-enhanced Raman spectroscopy (SERS)-based, colorimetric-based and infrared (IR)-based platforms.

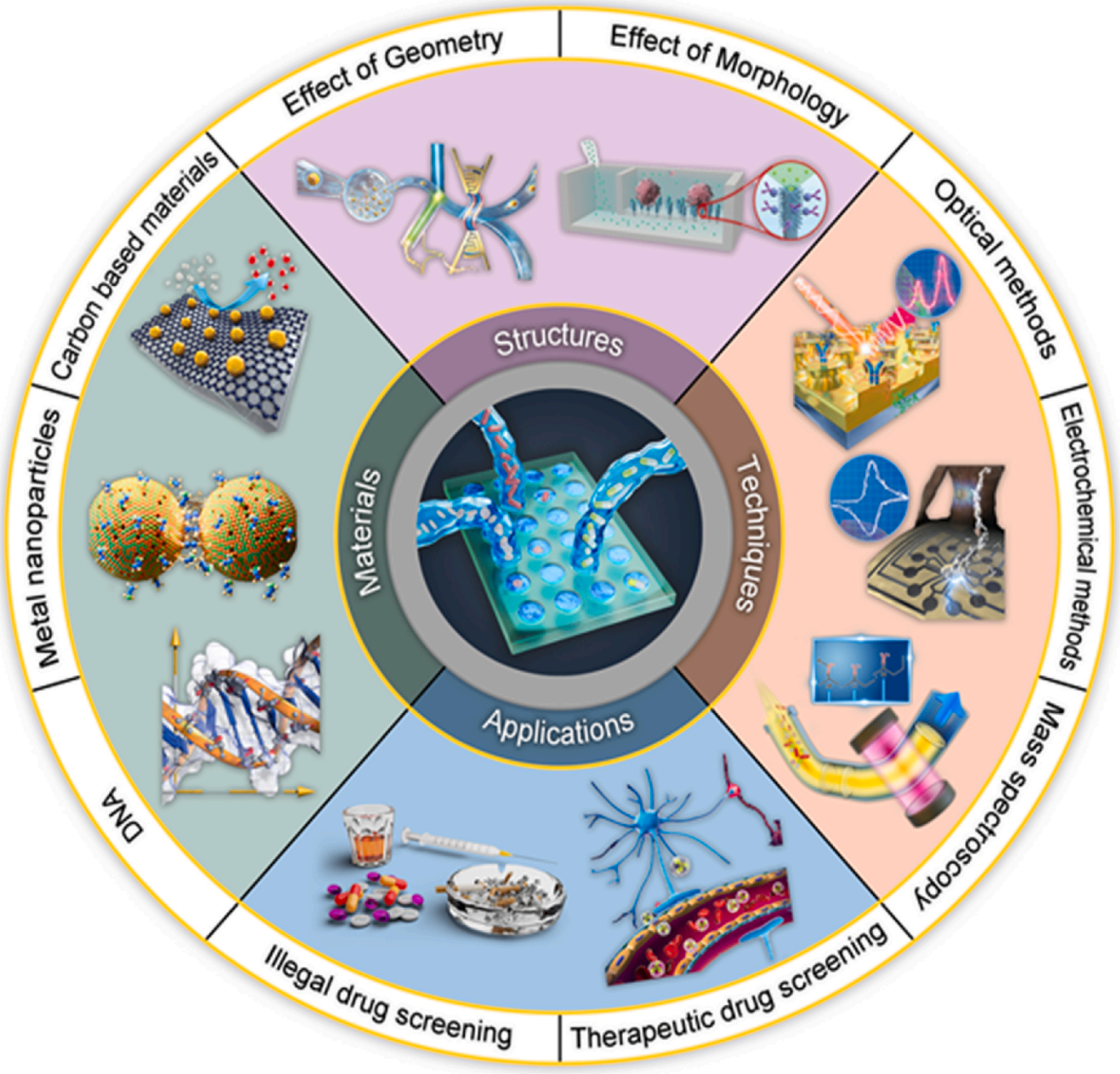

Fig. 1. Schematic representation of microfluidics-assisted drug sensing and screening techniques. The influence of sensing materials; gold nanoparticles, reproduced with permission from (Kim et al., 2014), copyright 2014 Wiley-VCH; graphene, reproduced with permission from (Song et al., 2022), copyright 2022 Wiley-VCH, and DNA, reproduced with permission from (Nummelin et al., 2018), copyright 2018 Wiley-VCH. The influence of surface morphology, reproduced with permission from (He et al., 2019), copyright 2019 Wiley-VCH, and geometrical designs, reproduced with permission from (Zhong et al., 2021), copyright 2021 Wiley-VCH. Drug screening and detection techniques; optical, reproduced with permission from (Liang et al., 2019; Yu et al., 2020), copyright 2019, 2020 Wiley-VCH, respectively; electrochemical, reproduced with permission from (Xu et al., 2021), copyright 2021 Wiley-VCH, and mass spectroscopy. Applications in therapeutic, reproduced with permission from (Wu et al., 2019), copyright 2019 Wiley-VCH, and illicit drug screening.

2.1.1. *Fluorescence-based platforms*

Overall, fluorescence is the predominantly utilized optical detection technique for drug screening in microfluidic devices owing to its high sensitivity and selectivity in small-molecule sensing (Liu et al., 2018; Mao et al., 2020). For the screening pharmacological compounds, different types of fluorophores, such as fluorescent dyes, proteins, and autofluorescent drugs, are used to generate fluorescent signals. This optical detection method utilizes a fluorophore to characterize the cell viability, lysis, and intracellular enzyme reactions in response to the drug molecules inside a microfluidic channel for screening applications. For instance, different types of cancer cells were cultured in a microfluidic chip in the presence of common autofluorescent anticancer drugs, such as doxorubicin (DOX) (Bandaru et al., 2019; Eilenberger et al., 2021; Tang et al., 2021), paclitaxel (PTX) (Lin et al., 2020; Schuster et al., 2020), cisplatin (CIS) (Eilenberger et al., 2021; Schuster et al., 2020), thiostrepton (TST) (Lin et al., 2020), and salinomycin (SAL) (Lin et al., 2020), and the half-maximal inhibitory concentrations (IC50 values) of the drugs were determined to screen the anticancer therapeutic agents. The results clearly showed that with increasing drug concentration, the viability of the cancer cells decreased, which was evidenced by the decrease in the fluorescence intensity of the drugs. Furthermore, several studies have reported that parameters such as drug flow rate and cell spheroid size strongly influence the fluorescence intensity, hence determining the screening sensitivity (Eilenberger et al., 2021; Tang et al., 2021). Interestingly, Lin et al., in 2020 also demonstrated the selectivity of drug screening platforms for anticancer drugs based on their fluorescence intensity by designing a single-cell clone forming inhibition assay for cancer stem cells (CSCs) (Lin et al., 2020). Nonselective drugs such as DOX and PTX showed an immediate effect on the viability of CSCs; however, selective drugs such as TST and SAL displayed latent effects. In addition to cancer drugs, fluorescence-based microfluidic devices with unique characteristic features have also been utilized for the screening of newer drug targets, such as nonhormonal contraceptives (Li et al., 2019), transient receptor potential (TRP)

channels (Ai et al., 2020), and protein receptor oligomers (Song and Jung , 2019). For instance, in 2020, Ai et al. proposed a single-cell trapping-based strategy for the screening TRP channel modulators that displayed superior screening performance compared to the conventional Flexstation 3 assay, which involved repeated compound administration (Fig. 2a) (Ai et al., 2020). The as-developed microfluidic method exhibits a significant decrease in false positives/negatives from 76.2% in conventional assays to 4.8% in Ca^{2+} fluorescence imaging due to the inclusion of single-cell heterogeneity during the screening process. In 2020, Schuster et al. demonstrated a combination drug against pancreatic tumor organoids: which were seeded in a microfluidic channel, and the drug exposure of the organoids was continuously monitored using live-cell imaging with fluorescent dyes to detect apoptosis and cell death (Fig. 2b) (Schuster et al., 2020). Moreover, to reduce the sample volume and improve throughput, droplet-based microfluidic sorters are becoming increasingly popular, and fluorescence detection is widely used to obtain signals for drug identification and screening (Hu et al., 2020; Paek et al., 2019; Zhong et al., 2021).

2.1.2. SERS-based platforms

Surface-enhanced Raman spectroscopy (SERS) is a type of vibrational spectroscopic technique that provides a unique molecular

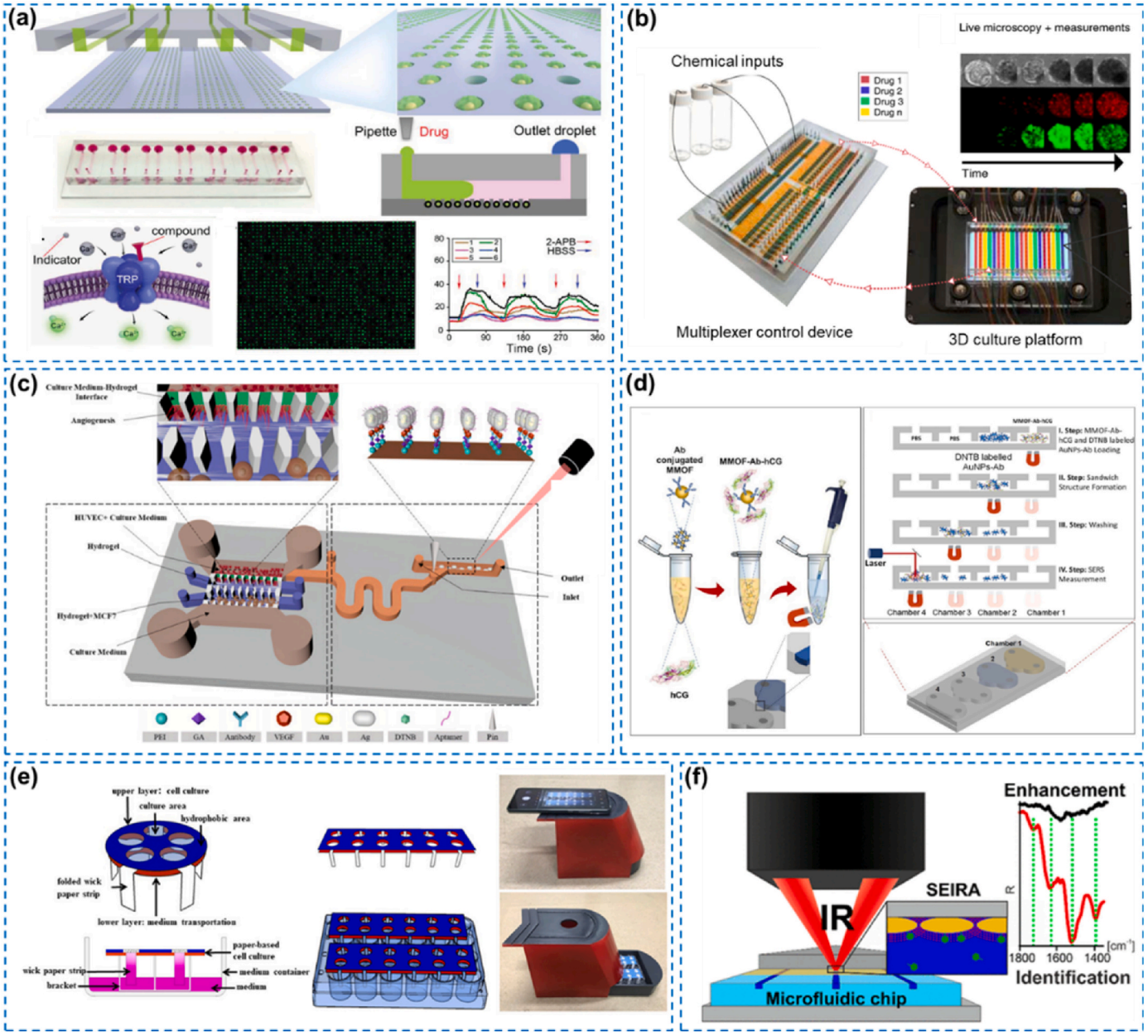

Fig. 2. Optical techniques for drug screening in microfluidic devices. (a) A fluorescence-based microfluidic device for the screening of TRPs, reproduced with permission from (Ai et al., 2020), copyright 2020 Wiley-VCH. (b) Combinatorial drug screening of anticancer drugs against tumor organoids based on on-chip fluorescence detection, reproduced with permission from (Schuster et al., 2020), copyright 2020 Nature Publishing Group. (c) A multifunctional microfluidic platform with SERS detection unit for the monitoring of different cytokines, reproduced with permission from (Qian et al., 2020b), copyright 2020 American Chemical Society. (d) A capillary-driven microfluidic chip for detection of hCG molecules in urine samples by employing a SERS detector, reproduced with permission from (Ahi et al., 2022), copyright 2022 Elsevier. (e) Paper-based microfluidic device with wick-like structure for colorimetric screening of anticancer drugs, reproduced with permission from (Fu et al., 2021), copyright 2021 Wiley-VCH. (f) Microfluidic chip integrated with in situ IR spectroscopy for highly sensitive screening of single molecules, reproduced with permission from (Kratz et al., 2018), copyright 2018 American Chemical Society.

fingerprint of the analyte of interest by relying on inelastic scattering of light (Andreou et al., 2013; Yue et al., 2022). Utilizing plasmonic nanostructures as substrates, SERS can achieve 8 times higher scattering cross-sections than traditional Raman spectroscopy, which allows Raman signal enhancement by a factor of 1010–1011, hence mediating single-molecule detection (Yue et al., 2022). Generally, plasmonic nanostructures and drug analytes are injected into microfluidic devices and undergo reaction within the channel, followed by integration of the stationary substrates into the chips. The SERS analysis is carried out on stationary substrates where the signal changes based on the drug concentration, hence enabling drug monitoring. For microfluidics-based drug screening, two strategies of SERS detection are usually employed: label-free and labeled detection. The label-free strategy relies on the direct absorption of drug molecules onto the SERS substrate to provide the Raman signal information of the drugs. To date, several plasmonic nanostructured substrates, such as gold nanoparticles (AuNPs), silver nanoparticles (AgNPs), Au/Ag core-shell nanostructures, and hybrid AgNPs, have been utilized as SERS probes for the detection of several drugs, such as illicit drugs and anticancer drugs (Koh et al., 2021; Qian et al., 2020a; Segawa et al., 2019; Sivashanmugan et al., 2019). Qian et al. developed a multifunctional microfluidic platform with a SERS detection unit for the detection of the cytokine VEGF by employing Au/Ag core-shell nanorods (NRs) labeled with the Raman reporter 5, 5′-dithiobis-2-nitrobenzoic acid (DTNB) as substrates (Fig. 2c) (Qian et al., 2020b). In addition, among all the detection methodologies, the SERS technique has shown promising results in the screening of drug analytes in real samples such as saliva, blood, urine, and sweat. For instance, Ahi et al. fabricated a capillary-driven microfluidics-based SERS detection platform for the analysis of human chorionic gonadotropin (hCG) protein in urine samples by using an antibody-modified magnetic metal-organic framework (MMOF) as the capture probe (Fig. 2d) (Ahi et al., 2022). Owing to their direct and noninvasive nature, wearable sensors based on SERS technology have recently been designed by integrating optically active plasmonic nanostructures onto flexible substrates. In 2021, Koh et al. reported a wearable SERS patch for the label-free detection of 2-fluoro-methamphetamine (2-FMA) in sweat which comprises of silk fibroin film (SFF) for the absorption of drugs from the skin surface and modification of the SFF with Ag nanowires (NWs) to generate SERS signals for the absorbed molecules under laser irradiation through the transparent dermal patch (DP) layer (Koh et al., 2021).

2.1.3. Colorimetric-based platforms

In recent years, colorimetric sensors have attracted tremendous attention for the screening of drugs outside clinical environments due to their cost-effectiveness, simplicity, and even visualization by the naked eye (Musile et al., 2021). Generally, colorimetric screening of drugs is carried out in paper-based microfluidic devices that are immobilized with specific probes, such as nanomaterials or enzymes, which results in a color-changing chemical reaction upon binding with the drugs (Ansari et al., 2017). Since the color change can be visible to the naked eye, colorimetric-based screening methodologies hold significant potential for instrument-free point-of-care testing (POCT). To date, different drugs, such as anti-neurological drugs (Liu et al., 2022), anticancer drugs (Fu et al., 2021), benzodiazepines (Ansari et al., 2017), and glucose (Ilacas et al., 2019), have been detected using colorimetric methods. For instance, in 2022, Liu et al. utilized the peroxidase-like activity of CeO_2–$Co(OH)_2$ nanosheets for the highly sensitive and selective detection of acetylcholinesterase (AChE) with a linear range of 0.2–20 mU/mL (Liu et al., 2022). The excellent catalytic performance of CeO_2–$Co(OH)_2$ nanosheets was related to the presence of oxygen vacancies. For instance, Ansari et al. designed a portable smartphone-integrated paper-based microfluidic device for measuring alprazolam (ALP) in vitreous humor and blood based on functionalization of AgNPs onto the paper which changed the color to reddish brown upon binding with ALP (Ansari et al., 2017). In another study, Fu et al., in 2021 fabricated an innovative wick-like paper-based microfluidic device for culturing 3D tumor cells to test the activity of anticancer drugs (Fig. 2e) (Fu et al., 2021). The results showed that the effect of the drugs on the cells was directly related to the color intensity, with lighter color intensity appearing on the paper at higher drug concentrations due to the lower cell viability.

2.1.4. Infrared-based platforms

In contrast to the other optical methods used for drug screening, IR-based spectroscopic techniques are label-free approaches that directly probe the unique vibrational fingerprint of drug molecules for their quantification (Gasper et al., 2009). Moreover, IR spectroscopy-based detection can generate the signal without time delay, is independent of the charge/polarizability of the sample and does not require complicated functionalization steps. For drug analysis, droplets of the drug solution in IR absorbing media are generated using the liquid–liquid extraction method, which is then transferred to an IR-transparent solvent equipped with waveguide IR spectroscopy for on-chip drug detection (Baker et al., 2014; Wägli et al., 2013). To enhance the sensitivity, microfluidic substrates are often functionalized with metal island films for signal enhancement, which is known as surface-enhanced IR spectroscopy (SEIR). For instance, in 2018, Kratz et al. proposed an optofluidic platform by integrating SEIR with microfluidics, which offers potential applications in drug screening by detecting the protein responses to particular drugs (Kratz et al., 2018). Along with the IR-transparent windows, a single-reflection geometry at an incidence angle below the attenuated-total-reflection (ATR) regime is employed, which reduces the strong IR absorption of common polymer materials and aqueous environments in the IR fingerprint region, allowing this configuration to be used for high-throughput drug detection (Fig. 2f).

2.2. Electrochemical techniques

Electrochemical (EC) biosensors have shown advantages such as simple instrumentation, high sensitivity, cost-effectiveness, easy integration, and miniaturization (Silvestrini et al., 2015). Hence, electrochemical microfluidic biosensors are frequently used in drug screening (Teymourian et al., 2020) and biomolecule detection (Lee et al., 2018; Tiwari et al., 2022). Here, we emphasize microfluidics-based drug sensing and screening based on electrochemical techniques such as electrochemical impedance spectroscopy (EIS), amperometry, cyclic voltammetry (CV), and differential pulse voltammetry (DPV). The integration of electrochemical techniques and microfluidic devices facilitates highly sensitive, noninvasive, low-volume, and label-free drug sensing and screening platforms.

EIS is a rapid technique used to study the kinetics of interfaces (Pejcic and DeMarco, 2006; Muñoz et al., 2017) in EC biosensors that estimate the loadings of immobilized bioreagents on the electrode surface by measuring the change in impedance (Sadik et al., 2009). Fig. 3a depicts an EC-based microfluidics biosensor for long-term monitoring of human organoids during drug toxicity studies. Herein, albumin (a representative biomarker of healthy liver tissue) and GST-α (a representative biomarker of acute liver injury) detection was based on EIS measurements. The amount of antigens captured on the functionalized electrode surface with antibodies, proportional to the antigens in the solution, was measured by measuring the impedance of the electrodes. The fabricated microfluidic sensor was capable of detecting albumin with an LOD of 0.09 ng mL^{-1} and a sensitivity of 1.35 (log (ng mL^{-1})) $^{-1}$, and the GST-α biosensor was found to detect up to 50 ng mL^{-1} with an LOD of 0.01 ng mL^{-1}. In this microfluidic platform, the cell secretum from the organoid flows automatically to the EC biosensor. Furthermore, this platform shows excellent capability for long-term drug toxicity monitoring before human trials by measuring the variation in albumin and GST-α (Shin et al., 2017).

Moreover, an EC-based microfluidic device has been used by Chawla

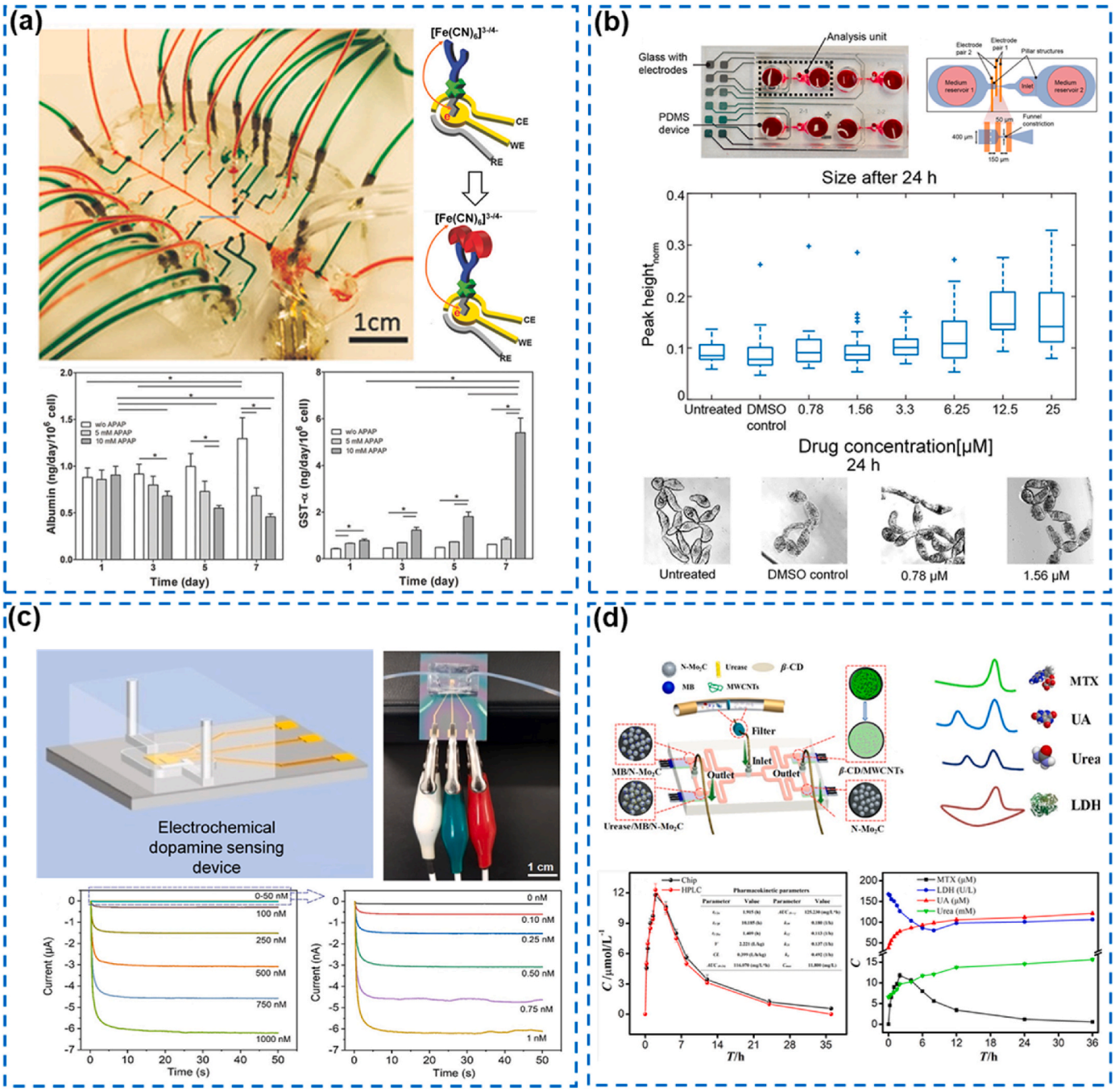

Fig. 3. Different electrochemical mechanism sensors integrated with microfluidics. (a) Label-free and regenerative electrochemical microfluidic biosensors for continual monitoring of cell secretum, reproduced with permission from (Shin et al., 2017), copyright 2017 Wiley-VCH. (b) Impedance-based microfluidic assay for automated antischistosomal drug screening, reproduced with permission from (Chawla et al., 2018), copyright 2018 American Chemical Society. (c) Microfluidic electrochemical sensor for cerebrospinal fluid and blood dopamine detection in a mouse model of Parkinson's disease, reproduced with permission from (Senel et al., 2020), copyright 2018 American Chemical Society. (d) Application of multiplex microfluidic electrochemical sensors in monitoring hematological tumor biomarkers, reproduced with permission from (Zhu et al., 2020), copyright 2018 American Chemical Society.

et al. to study the mortality of schistosomiasis (a tropical disease caused by parasitic worms). Herein, EIS measurements have been employed to monitor the variation in impedance of two different groups of electrodes, where one group of electrodes reveals the number and size, and the other group of electrodes reveals the precise mortality of worm larvae to estimate their viability (Fig. 3b). The multiplexing of the analyzed units allowed us to simultaneously record changes in the motility of larvae exposed to different drug concentrations in different analysis units without disturbing the signal between different units. Compared to a trained operator's phenotypic evaluation of the worm larvae using manual microscopy, automated assessment by the microfluidic platform provides an excellent correlation to view scores (Chawla et al., 2018).

Amperometry has been utilized with a microfluidic device by Weltin and coworkers to monitor glucose and lactate secretion from cancer cells. This platform has been used for long-term and online dynamic monitoring of recovery after applying a drug (cytochalasin B) to cancer cells. Cytochalasin B (CB) is a commonly used compound that blocks glucose and lactate metabolism inside the cell. By applying CB to the cultured cells, the direct effect of the change in the extracellular

concentration of glucose and lactic acid can be observed by the amperometry-based microfluidic platform (Weltin et al., 2014). In addition, Senel et al. employed amperometry with a microfluidic platform for dopamine (DA) detection. The developed microfluidic device is depicted in Fig. 3c, which shows a linear current response from 0.1 to 1000 nM for DA concentrations in phosphate buffered saline (PBS) and aCSF (artificial cerebrospinal fluid). This integrated platform has shown the potential to improve DA detection after treatment with L-3,4-dihydroxyphenylalanine (L-dopa) in patients with Parkinson's disease (Senel et al., 2020). Moreover, some groups combined different electrochemical techniques with microfluidic platforms for multiple analyte detection. Interestingly, Zhu et al., in their system, employed pulsed voltammetry to screen methotrexate (MTX), urea, and uric acid (UA). Moreover, lactate dehydrogenase (LDH) was detected by cyclic voltammetry. Fig. 3d shows a schematic of the microfluidic platform that employed different electrochemical techniques to detect multiple analytes on a single chip (Zhu et al., 2020).

2.3. Mass spectrometry

Mass spectrometry (MS) is a method for measuring charged ions and consists of three main components: an ion source, a mass analyzer, and a detector. The basic principle of mass spectrometry is that the ion source is generated by freeing the sample from the molecular state to the charged ion state through high temperature, plasma, and laser irradiation. Then, the charged ions are accelerated by the high pressure and

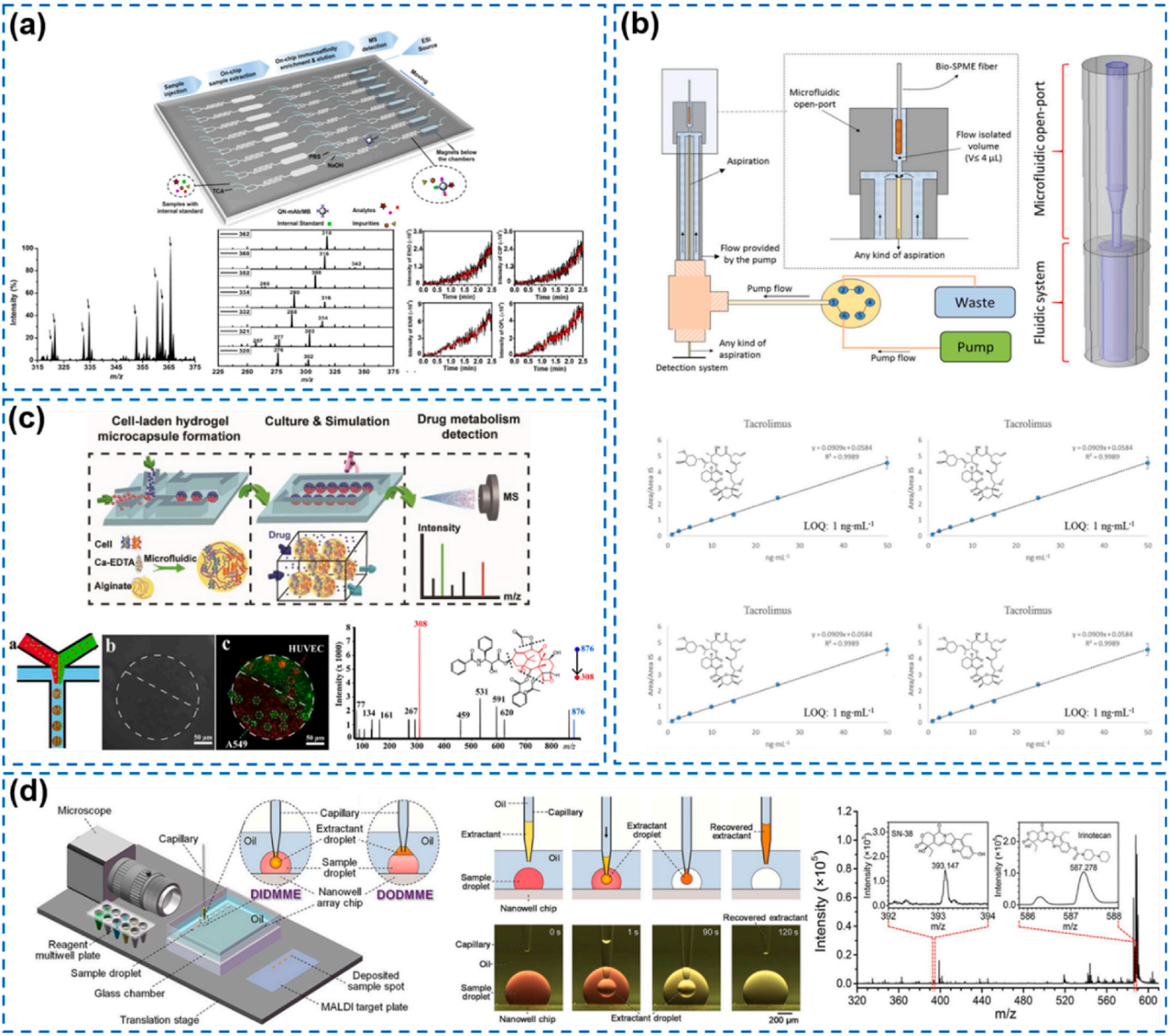

Fig. 4. Mass spectrometry techniques for drug screening in microfluidic devices. (a) Integrated microfluidic device coupled to mass spectrometry for the analysis of residual quinolones in milk, reproduced with permission from (Zhao et al., 2019), copyright 2019 American Chemical Society. (b) Coupling of Bio-SPME devices with MS for the analysis of immunosuppressive drugs, reproduced with permission from (Tascon et al., 2018), copyright 2018 American Chemical Society. (c) An integrated microfluidic chip coupled to mass spectrometry to probe drug resistance in a tumor-endothelial coculture model, reproduced with permission from (Zheng et al., 2020), copyright 2019 Elsevier B.V. on behalf of the Chinese Chemical Society and Institute of Materia Medica, Chinese Academy of Medical Sciences. (d) A rapid and flexible droplet–droplet microfluidic microextraction system for metabolite analysis of cell droplets, reproduced with permission from (Sun et al., 2020), copyright 2020 American Chemical Society.

passed into the mass analyzer of the mass spectrometer. Under the action of external physical forces such as electric and magnetic fields, the detector can measure the mass-to-charge ratio of different ions, and the mass of the analyte can be deduced from the charge. Therefore, mass spectrometry can be used for the identification or confirmation of molecules (Domon and Aebersold, 2006; Sansa et al., 2020). The integration of microfluidics with mass spectrometry provides a simple and sensitive analytical workflow process (Kazoe et al., 2021; Liu and Lin, 2016; D. Zhang et al., 2021) with automation capability, reduced sample preparation (Liu and Lin, 2016), shorter analysis time (Korzhenko et al., 2021), good reusability, high throughput (Looby et al., 2019), high characterization capability (Shen et al., 2021), and easy integration with various isolated instruments (Spencer et al., 2022), thus greatly enhancing the analytical capability. Herein, the integration of mass spectrometry and microfluidics is ideally suited for highly sensitive drug screening. Drug screening covers a wide range of topics, including the retention of antibiotics in food (Wu et al., 2016; Zhao et al., 2019), monitoring of blood levels of therapeutic drugs for clinical diagnosis (Kazoe et al., 2021b; Korzhenko et al., 2021b; Spencer et al., 2022b; Tascon et al., 2018), and screening of anticancer drugs (Lin et al., 2016b; Sun et al., 2020; Wu et al., 2016b).

In this regard, Zhao and coworkers have developed an immunoaffinity microfluidic chip combined with an electrospray ionization–mass spectrometry (ESI–MS) platform for the qualitative and quantitative analysis of antibiotic residues in milk matrices, as shown in Fig. 4a. A single isotope internal standard method for the quantitative analysis of seven quinolones was proposed. After extraction and enrichment with antibody-coupled magnetic beads, the seven quinolones were specifically extracted and quantified with a linearity range of 0.2/0.5–10 ng/mL ($R^2 > 0.991$). The LODs for the seven quinolones were in the range of 0.047–0.490 ng/mL (Zhao et al., 2019).

Furthermore, for therapeutic drug sensing and screening in blood samples, Tascon et al. proposed a new method using a microfluidic design to facilitate direct coupling of biocompatible solid-phase microextraction (Bio-SPME) devices with MS, as shown in Fig. 4b. The design was applied to an ESI-MS/MS system for experimental validation. The results showed the rapid determination of selected immunosuppressive drugs (e.g., tacrolimus, cyclosporine, sirolimus, and everolimus) from 100 μL whole blood samples. The limits of quantification for all compounds studied were within the sub-ppb range with excellent sensitivity. Good linearity ($R^2 \geq 0.99$) and excellent precision were obtained with and without internal standard correction (Tascon et al., 2018b). Zheng et al. designed a microfluidic chip platform to construct a three-dimensional tumor-endothelial coculture model to simulate drug resistance during tumor treatment, as depicted in Fig. 4c. The anticancer drug paclitaxel was selected as the model. The experimental results showed that the cells maintained high viability in the 3D dynamic microenvironment, confirming the good biocompatibility of the platform. However, on-chip culture enables continuous drug stimulation, and significant differences in drug uptake between monoculture and coculture models can be clearly observed (Zheng et al., 2020). Fig. 4d depicts a droplet-in-droplet microfluidic microextraction platform to perform nanoscale microsample pretreatment by combining droplet-based microfluidics, robotic liquid handling, and liquid-phase microextraction technology. The advantage of the system is that the sample volume can be reduced to the nanoliter level, and the extraction time can be shortened by 10–20 times. The microextraction system was combined with matrix-assisted laser desorption/ionization-time of flight (MALDI-TOF) mass spectrometry for the screening of SN- 38, the active metabolite of the anticancer drug irinotecan. For this platform, a linear relationship in the range of 4–100 ng/mL ($R^2 = 0.984$) was obtained in 800 nL droplets containing HepG2 cells, with a detection limit of 2.2 ng/mL and a quantification limit of 4.5 ng/mL for SN-38 (Sun et al., 2020b). Table 1 provide a comparison of sensing performances based on different types of sensing techniques used for drug screening and sensing.

3. Materials

3.1. Materials for sensing

Numerous types of materials have been used for screening and sensing of illicit drugs, metabolites, pathogens, DNA, and cells in the microfluidic devices (Chen et al., 2021; Lin et al., 2016; Sengupta and Hussain, 2019). In particular, in the case of microfluidic device-based drug sensing, most of the utilized materials are carbon and its derivatives, metal nanoparticles, DNAs, aptamers and hybridized materials combined with various techniques. These materials have shown their potential for specific and efficient sensing with modification by different functional groups (Ansari et al., 2016; Chen et al., 2018a; Dutse and Yusof, 2011; Naresh and Lee, 2021).

3.1.1. Carbon-based materials for sensing

The carbon-based materials (reduced graphene oxide (rGO), multi-walled carbon nanotubes (MWCNTs), single-walled carbon nanotubes (SWCNTs) and carbon quantum dots (CQDs)) have shown potential for microfluidic device-based screening of various types of analytes and drugs (Chen et al., 2018b; Materón et al., 2018; Tung et al., 2017; Walther et al., 2020; Wee et al., 2019). The potential of these materials for biosensing may be attributed to their unique properties, such as the excellent optical properties of CQDs, flexibility, the high electron mobility and photothermal property of graphene, and the high surface area and high electrical conductivity of CNTs (Li et al., 2017; Soldano et al., 2010; Wang and Hu, 2014). In a study of cardiac sensing and evaluation based on a heart-on-a-chip-based microfluidic device, rGO hybridized color film with anisotropic morphology was combined with a heart-on-a-chip system (Li et al., 2020). For the construction of the anisotropic color film, rGO-modified GelMA hydrogel and polyethylene

Table 1
Comparison of sensing performances among different detection techniques for sensing and screening of drugs.

Detection Technique	Target analyte	Linear range	LOD	Reproducible	Refs.
Optical	Formaldehyde	40 μM–266 μM	7 μM	Yes	Liu et al. (2018)
Optical	DOX	1.8 μM–12.9 μM	1.3 μM	Yes	Tang et al. (2021)
Optical	Cisplatin	1 μM–500 μM	–	Yes	Eilenberger et al. (2021)
	DOX	1 μM–500 μM	–		
Optical	Methamphetamine	67 μM–3.4 mM	67 μM	Yes	Koh et al. (2021)
Electrochemical	GST-α	–	0.2 pM	Yes	
	Albumin	1.5 pM–1.5 nM	0.15 pM		Shin et al. (2017)
Electrochemical	Mefloquine	0.78 μM–25 μM	0.78 μM	Yes	Chawla et al. (2018)
Electrochemical	Dopamine	0.1 nM–1 μM	0.1 nM	Yes	Senel et al. (2020)
Electrochemical	Methotrexate	0.1 μM–1000 μM	35 nM	Yes	Zhu et al. (2020)
Mass spectroscopy	Quinolones	0.6 nM–29.5 nM	0.1 nM	Yes	Zhao et al. (2019)
Mass spectroscopy	SN-38	10 nM–255 mM	5.6 nM	Yes	Sun et al. (2020)

glycol diacrylate (PEGDA) pregel were used with the microgroove surface morphology of GelMA, as shown in Fig. 5a. When this anisotropic hydrogel film was integrated into the microfluidic device and cardiomyocytes were assembled on the GelMA film, due to their autonomous beating, they exhibited contraction and relaxation, which changed the structural color of the film. Moreover, this structural color change property with the beating action of cardiomyocytes was utilized to study the effect of isoproterenol on cardiac contractility. As shown in Fig. 5a, with increasing isoproterenol concentration, an increase in structural color change was detected.

A study has been reported based on a novel trimodal system in which ketamine was detected with three types of mechanisms with three different types of sensing regions, as shown in Fig. 5b (Yehia et al., 2020). In this work, CQDs were employed as fluorescent sensing materials in combination with gold nanoparticles (AuNPs). The synthesized CQDs had an average particle size of 8 nm and showed intense photoluminescence at 453 nm (blue luminescence) and 519 nm (green luminescence) upon excitation at 350 nm and 400 nm, respectively, as shown in Fig. 5b. Moreover, CQDs-based fluorescence sensing showed a ketamine concentration-based fluorescence change (blue to purple), and further analysis revealed that the intensity of red light of the fluorescent signal was linearly related to the concentration of ketamine in the range from $2 \times 10^{-4} - 1 \times 10^{-3}$ mol/L. In another study of screening of dopamine, sodium dodecyl sulfate (SDS) surfactant-modified graphene was used as the sensing surface (Manbohi and Ahmadi, 2019). In this study, the microfluidic sensing system was fabricated by using chromatography paper and low-cost wax-based stamping to make a hydrophobic surface, which was not used as a sensing circular area (Fig. 5c). Moreover, the sensing performance of CNT-based sensors, Fe_3O_4-based sensors and SDS surfactant-modified graphene-based sensors for dopamine has been tested, and all of them showed sensitivity toward dopamine. However, in the presence of uric acid and ascorbic acid, the SDS surfactant-modified graphene-based sensor showed both sensitive and selective detection of dopamine concentration changes with a linear range from 0.5 μM to 120 μM and an LOD of 0.01 μM, as shown in Fig. 5c. In accordance with the above discussion, it can be said that carbon and its derivative-based materials exhibit numerous advantages in the fields of biosensing and screening (Singh et al., 2022).

3.1.2. *Nanoparticle-based materials for sensing*

Nanoparticles possess unique physical and chemical properties along with their wide range of sizes of 1–100 nm. Moreover, the sizes of nanoparticles are comparable to the dimensions of antibodies, metabolites, membrane receptors, nucleic acids and proteins. These biomimetic functions, along with their large surface area: volume ratio and the potential of tuning their properties, make nanoparticles a unique and powerful tool for imaging, screening, and diagnosis (Pison et al., 2006; Sanvicens and Marco, 2008; Yezhelyev et al., 2006). In particular, metal nanoparticles such as Au, Ag, Ni, Pt and TiO_2 nanoparticles have shown potential in the field of biosensors such as microfluidics-based biosensors, TENG-based biosensors and electrochemical biosensors (Chatterjee et al., 2020; Choi et al., 2016; Pal et al., 2020; Pao et al., 2021; Rezvani Jalal et al., 2021; Xie et al., 2017). Especially, AuNPs (<50 nm) can be synthesized with various geometries, such as spheres, shells, rods, or cages in the nanodomain. These nanoparticles exhibit a localized surface plasmon resonant function when irradiated with light. AuNPs are excellent labels for biosensing because they are detectable by a number of techniques, such as optical absorption, fluorescence, and electric conductivity (Huang et al., 2007). Here, we focus on AuNPs as drug sensing materials in microfluidic devices.

In a study of phenol detection, a low-cost and simple microfluidic system was integrated with an electrochemical electrode that has a gold nanoparticle-multiwalled carbon nanotube (AuNP/MWCNT) composite on the surface, modified with tyrosinase (Caetano et al., 2018).

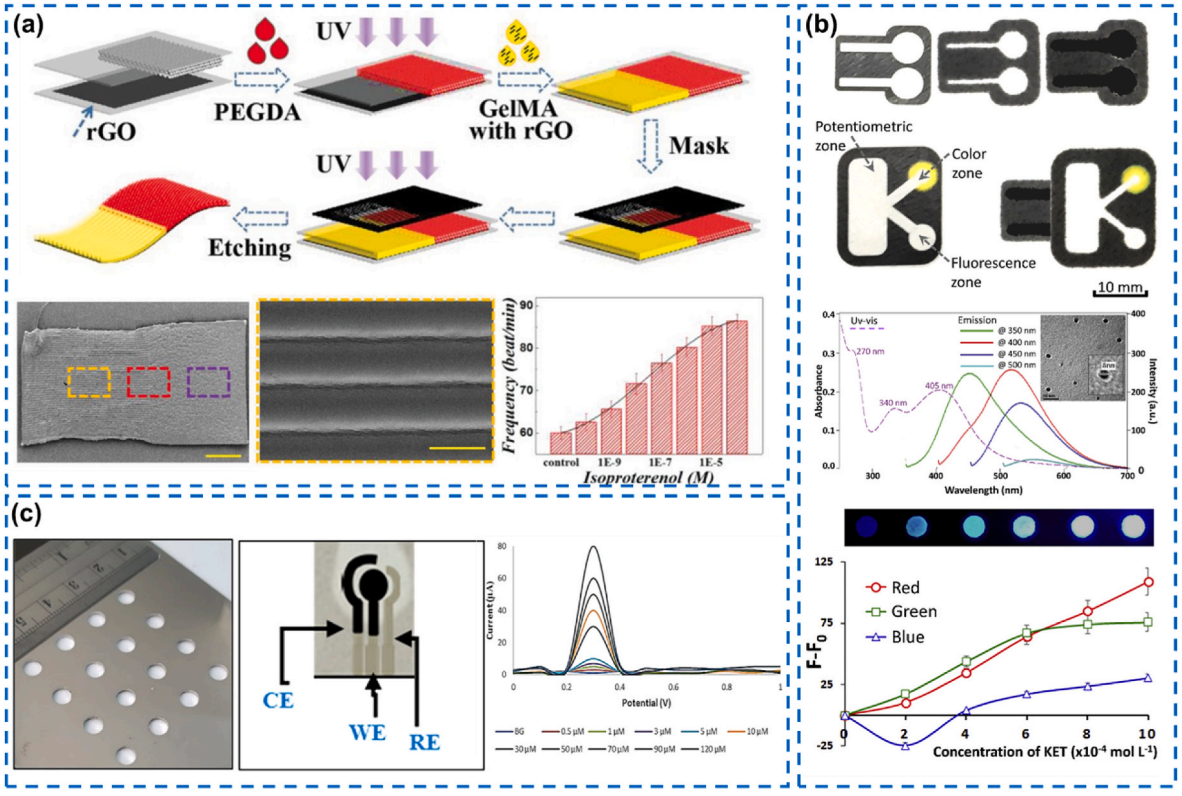

Fig. 5. Carbon derivatives as sensing materials in microfluidic devices. (a) rGO hybrid anisotropic structural film with multiple colors for cardiac sensing and analysis, reproduced with permission from (Li et al., 2019), copyright 2019 Wiley-VCH. (b) A novel trimodal system, where carbon quantum dots are used for fluorescent sensing, reproduced with permission from (Yehia et al., 2020), copyright 2020 Elsevier. (c) Microfluidic detection of dopamine through an electrochemical method based on graphene, reproduced with permission from (Manbohi and Ahmadi, 2019), copyright 2019 Elsevier.

Synthesized AuNPs in this study have a particle size of 7 ± 4 nm, which exhibits several sites for enzyme immobilization, and these AuNPs are well distributed on MWCNTs, as shown in Fig. 6a. When phenol-containing liquid starts to flow from the inlet reservoir to the outlet reservoir, the phenol molecule present in solution reacts with tyrosinase modified on the AuNP/MWCNT nanocomposite and forms o-quinone. Furthermore, this o-quinone undergoes electrochemical reduction, which changes the amperometric signals. The fabricated low-cost microfluidic device shows a linear range of phenol detection from 10 to 200 nmol L^{-1} with an LOD of 2.91 nmol L^{-1} and a high sensitivity of 131 nA μmol L^{-1}. Thus, the analysis of the proposed device shows the realization of phenol detection in simple and fast mode with low cost (Fig. 6a). A study has been reported for the detection of illicit drugs such as morphine, cocaine, and methamphetamine, where AuNPs and silver nanoparticles (AgNPs) are incorporated as SERS media. In this study, the materials and sizes of nanoparticles were optimized for the detection of the abovementioned illicit drugs based on SERS technology (Kline et al., 2016). Moreover, the interfaces of caping agents used for nanoparticles have also been studied, and among borate, tannate, and citrate, borate showed the best sensing performance. The synthesized AuNPs and AgNPs had particle sizes ranging from 20 nm to 80 nm. Moreover, these NPs showed size-dependent UV–vis absorption from 520 nm to 550 nm for AuNPs and from 390 nm to 460 nm, as shown in Fig. 6b. The SEM image of borate-capped AuNPs in Fig. 6b shows the purity and uniform size distribution of the particles. After optimization of the nanoparticle material and size, it was concluded that AuNPs (30 nm size) showed the best sensing performance, and the LODs measured for the methamphetamine, morphine, and cocaine target analytes were in the range of (1.5–4.7) × 10^{-8} M (4.5–13 ng/mL), as shown in Fig. 6b.

Nucleic acids modified with hybrid graphene oxide gold nanoparticle (Au@GO NPs) have shown great potential for accurate diagnosis and therapeutics. A study has reported a decrease in breast cancer cell (MDA-MB-231) viability based on Au@GO NP-induced hyperthermia with the combinatorial effects of doxorubicin and BCL2 suppressor (Yang et al., 2021). In this report, the hydrophobic interaction of iRGD-conjugated lipid ligands with GO and the bonding nature of

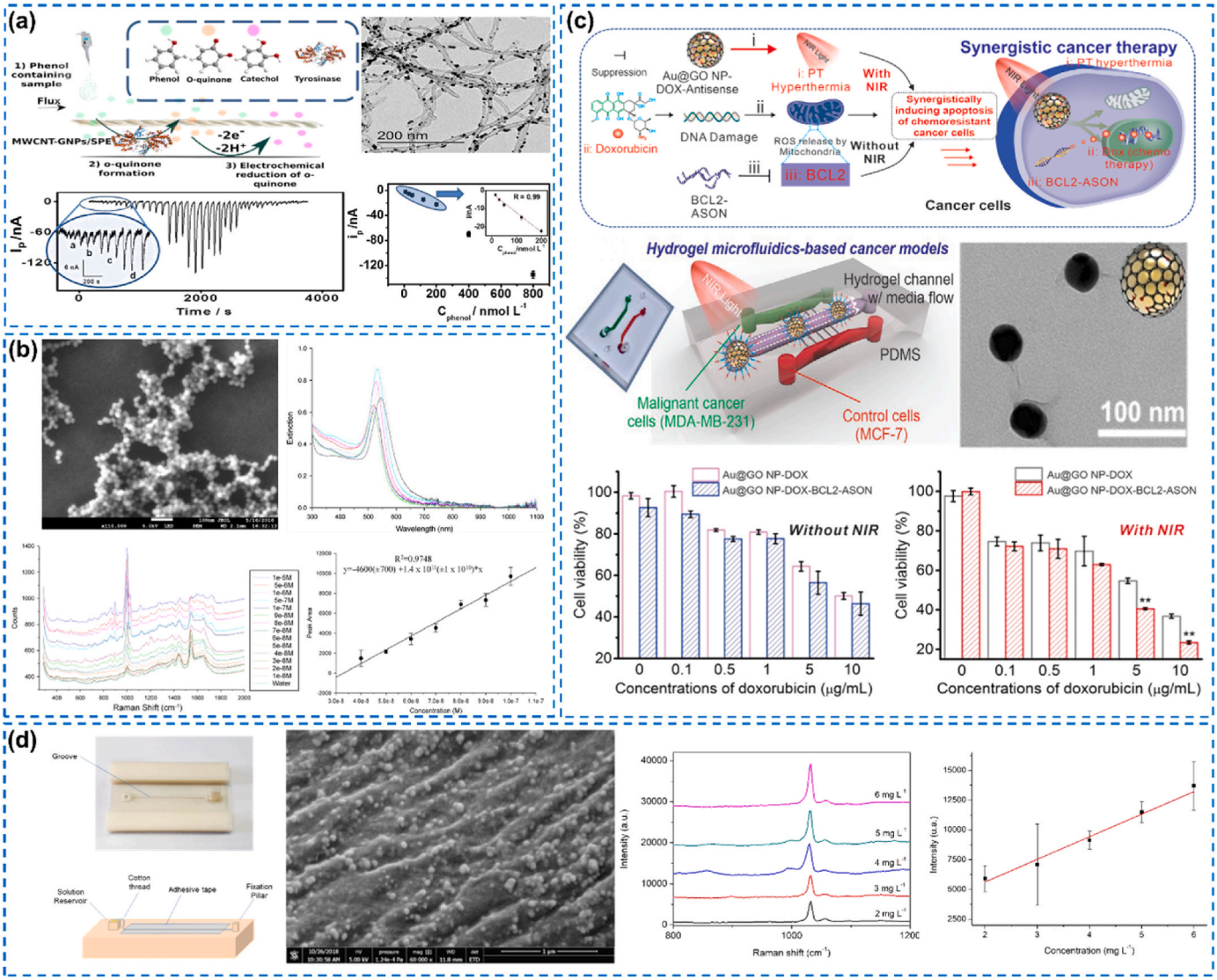

Fig. 6. Microfluidic drug sensing based on metal nanoparticles. (a) Phenol detection based on a combination of a commercial textile thread-based microfluidic device with a MWCNT/AuNP-modified electrode, reproduced with permission from (Caetano et al., 2018), copyright 2018 Elsevier. (b) Detection of methamphetamine, cocaine and morphine based on borate capped AuNPs in a microfluidic channel with the SERS technique, reproduced with permission from (Kline et al., 2016), copyright 2016 American Chemical Society. (c) Imaging of cancer apoptosis based on hybrid graphene-gold nanoparticle-based nucleic acid and doxorubicin, reproduced with permission from (Yang et al., 2021), copyright 2021 Wiley-VCH. (d) Synthesis of gold nanoparticles on textile threads for nicotine detection in microfluidic devices, reproduced with permission from (Adamo et al., 2020), copyright 2020 Elsevier.

iRGD-conjugated lipid ligands with $\alpha v\beta_3$ integrins on the surface of cancer cells have been utilized for selective cancer cell killing, as shown in Fig. 6c. Moreover, Au@GO NPs help to enhance the effect of hyperthermia, increase the anticancer toxicity of DOX and inhibit the overexpressed BCL2 gene. Most importantly, Au@GO NP-BCL2-NAC combined with NIR hyperthermia induced a significantly higher percentage of cell killing (approximately 31%) than the control groups of the ASON only with a 10 μg mL^{-1} loading concentration of DOX (Fig. 6c). Measurement of cancer cell viability also shows a decrease with increasing DOX concentration, as shown in Fig. 6c. In another study, nicotine detection was realized with a low-cost and rapid microfluidic device constructed by using cotton threads (Adamo et al., 2020). In this regard, gold nanoparticles were synthesized with the use of cotton thread and reagents ($HAuCl_4$ and $Na_3C_6H_5O_7$). The synthesized AuNPs have a diameter ranging from 20 nm to 40 nm, as shown in Fig. 6d. These synthesized AuNPs on cotton threads showed high sensitivity to a nicotine-containing solution with the SERS technique. Moreover, this AuNP-based system showed a linear sensing response for a concentration range of 2–6 mg L^{-1} with an LOD of 0.18 mg L^{-1}, as shown in Fig. 6d. From the above discussion, gold nanoparticles are proven to be ideal candidates for drug sensing in microfluidic devices due to the novel properties of this material.

3.1.3. DNA and aptamer-based materials for sensing

Deoxyribonucleic acid (DNA) sequences are specific for sensing and play a significant role in clinical diagnostics, food safety analysis, biosensing and biodefense applications (Das et al., 2012; Wu et al., 2014). DNA molecules exhibit unique self-recognition functions, offering higher flexibility and accessibility to exquisite nanostructures built "bottom-up" with ultrahigh controllability and precision. Moreover, DNA has natural conjugation properties with antibodies (Pei et al., 2011).

Detection of bisphenol A (BPA) has been performed in graphene field effect transistor integrated microfluidic devices where a graphene substrate is functionalized with double strained complementary DNA (dsDNA) (Liu et al., 2018). In this report, a solution-gated graphene transistor (SGGT) is constructed on a glass substrate covered with a PDMS channel. The graphene channel was functionalized with AuNPs with an average size of 30 nm, as shown in the TEM image of single-layer graphene in Fig. 7a. Moreover, this AuNP-modified graphene channel was modified with probe dsDNA molecules immobilized on the AuNPs, as shown in Fig. 7a. With the application of BPA solution, the transfer characteristics of SGGT changed, and these changes were consistent with the change in the concentration of BPA, with a linear response in the range of 10 to 5 × 10^4 ng/mL. In another study, DNA tetrahedron and aptamer-based aggregation induced the emission of luminescence, and these aggregated molecules were further modified with the anticancer drug DOX. Moreover, these modified molecules were attached to the surface of the graphene oxide layer, and the resulting sensing platform possessed higher selectivity for liver cancer cells (Ma et al., 2021). As shown in Fig. 7b, four ssDNAs were initially assembled by themselves to produce a DNA-tetra structure and further modified with hairpin switch aptamers followed by loading of the anticancer drug DOX on the DNA-tetra skeleton, as shown in Fig. 7b. Doxorubicin showed green fluorescence when it was added to the DNA-tetra skeleton, and to enhance this fluorescence, DASI, which is a fluorescent probe molecule

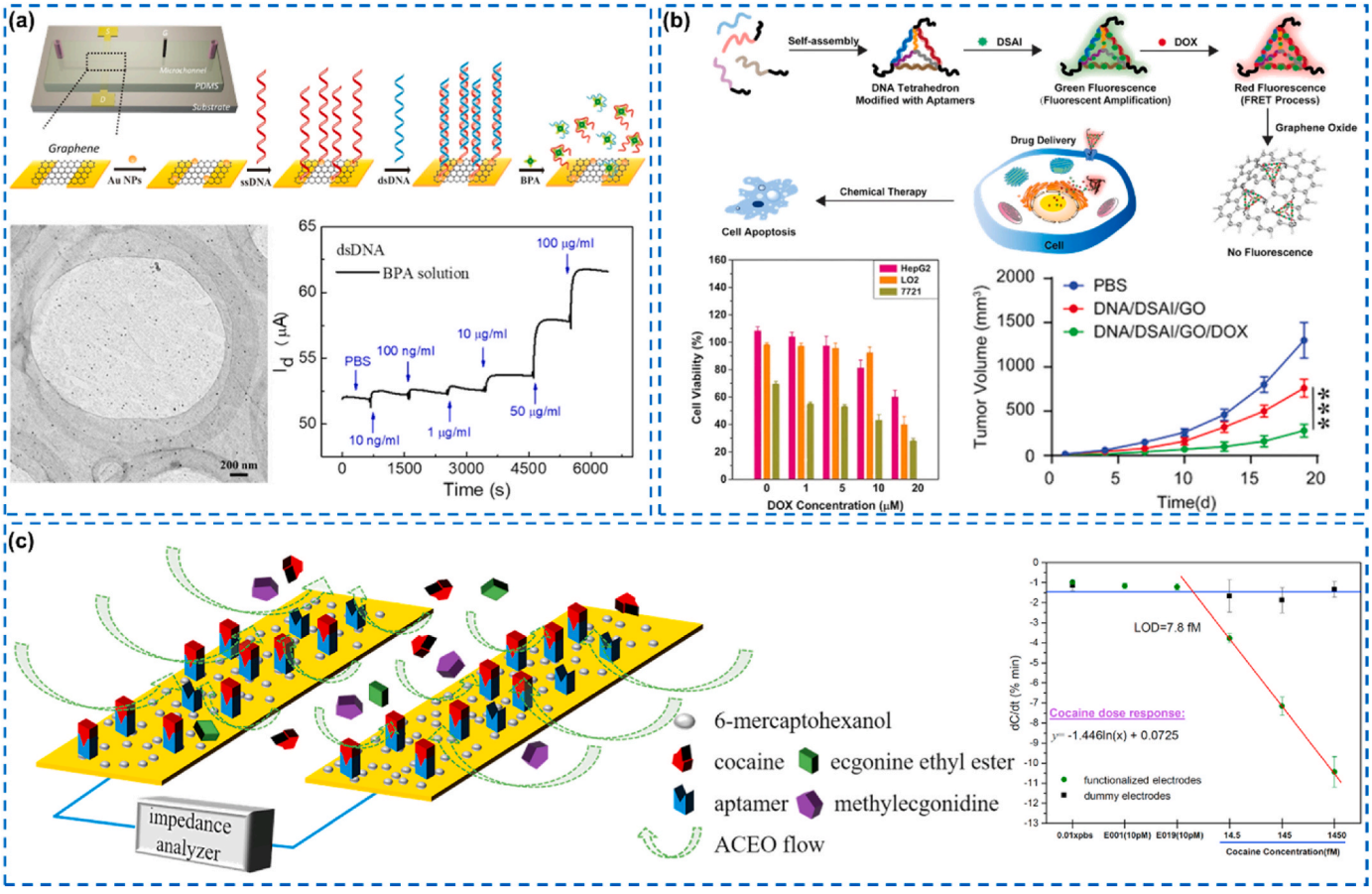

Fig. 7. DNA-based drug sensing with microfluidic devices. (a) Screening of bisphenol A based on DNA functionalized graphene with microfluidic device, reproduced with permission from (Liu et al., 2018), copyright 2018 American Chemical Society. (b) DNA-modified graphene oxide-based microfluidic for the diagnosis and treatment of liver cancer cells, reproduced with permission from (Ma et al., 2021), copyright 2021 Wiley-VCH. (c) Detection of serum cocaine based on aptamer-modified microfluidic system, reproduced with permission from (Oueslati et al., 2018), copyright 2018 Elsevier.

with aggregation-induced emission (AIE), was also loaded on the DNA structure, followed by the FRET process to produce bright red fluorescence, as shown in Fig. 7b. Moreover, the loading capacity of DOX, DASI and GO was optimized, and as shown in Fig. 7b, cell viability decreased with increasing DOX concentration. A comparative in vivo study was also performed to prove the efficiency of the fabricated DNA nanomaterials.

Cocaine is a highly intensive stimulant widely abused as a drug. A microfluidic device has been developed for screening cocaine in serum based on aptamers as probe molecules (Oueslati et al., 2018). In this work, the change in capacitance of the sensing surface in response to selective binding of cocaine on probe aptamer molecules was measured, as shown in Fig. 7c. Moreover, an alternative current was applied to induce rapid transportation of target molecules and prevent the influence of the matrix. The fabricated microfluidic device possesses properties such as low cost, rapid, and high selectivity. Moreover, in standard buffer solution, it shows a linear response in the range of 14.5 fM to 14.5 pM with a 7.8 fM LOD and a 30 s sample-to-result time. Moreover, in serum samples, this sensing platform show a 13.4 fM LOD, as shown in Fig. 7c. It can be concluded that materials based on carbon and its derivatives, metal nanoparticles and DNA-based nanomaterials exhibit numerous novel properties that have great potential for biosensing in microfluidic devices. Table 2 shows effect of different type of sensing materials on sensing properties of microfluidic sensors.

3.2. Materials for microfluidic platform fabrication

The surface properties of fabrication materials dominant significantly when it comes to microscale and these surface properties can either own to realization of unique properties or lead to problems. To realize individual functions, special attention is required for the selection of proper fabrication material, since it will decide the inherent properties of microfluidic device. In the past three decades, several types of materials have been employed in microfluidics. Initially, silica and glass were used in the fabrication of microfluidic devices. However, silica and glasses are hard which hinder their broad applications, expensive in fabrication, requirement of high-level protection, difficulties in bonding of chips and difficulties in creation of effective valves. Hence, by considering these problems, researchers have been used elastomers (like: PDMS) in abundance. This abundant use of PDMS owing to its properties like stretchability, compressibility, easy and low-cost fabrication, low curing temperature (40-70 °C), and ability of casting in nanometer resolution owing to its low surface tension. Moreover, PDMS allow integration of valves with high density, gas permeable, and biocompatible (Ren et al., 2013).

Other materials, like hydrogels are also good candidate for biomedical research and biomimicking, like study of cell culture in tissue-level and delivery of cell and solutions. Hydrogels are highly aqueous (water >90%), similar to extracellular matrix, highly biocompatible, and highly porous with controllable pore size. On other hand, paper-based devices have shown their potential towards microfluidics as these devices don't need to be sealed. Moreover, high porosity of paper (consist of cellulose), low-cost and very simple device fabrication, ease of storage, large surface-to-volume ratio, good capacity of wicking liquids, and ease of multilayer device fabrication are the properties which makes them suitable for drug sensing and screening (Derda et al., 2011).

4. Geometries and morphologies of microfluidic platforms

4.1. Geometries of microfluidic platforms

During the last decade, microfabrication technologies have led to the development of microfluidic channels with increasingly advanced geometrical designs. The development of different geometrical structures of the microfluidic channels enhances the sensing capability of these systems for drug screening. In addition, the significant advantage of microfluidics-based drug screening is the high-throughput or high-content analysis capability. The primary task in developing microfluidic systems for drug screening is to fabricate microfluidic devices based on the target's function (Regnault et al., 2018). For example, to inspect bimolecular gradients by guiding biological processes within dynamic circumstances and high-throughput chemical gradients (toxic substances or drugs), a microfluidic concentration gradient generator (MCG) is needed to obtain a platform with high stability for drug screening and chemotaxis for microorganisms or cells (Ahmed et al., 2010). The 'Christmas tree' is the classical geometrical design (Jeon et al., 2000) of MCG, in which the diffusion mixing principle of laminar flow comes to play. Furthermore, the design of the gradient generator should be compatible with other microfluidic functional components to provide adequate performance. For instance, Huanhuan et al., in 2019 designed an innovative MSG system capable of accumulating highly linear concentrations regardless of the flow rate. It was achieved by introducing a serpentine mixing channel to the MSG to initiate the mixing of the laminar flow in a much shorter length, as depicted in Fig. 8a (Shi et al., 2019). In addition, different geometrical designs facilitate the mimicking of human organs for drug screening in microfluidic systems. These can be engineered so that the cells can be adequately close (100–200 μm) to the supplied nutrients and oxygen to assure cell viability (Laschke et al., 2006), which can help to achieve appropriate physiological conditions for drug screening, tissue engineering (Choi et al., 2007), and vascularization (Jain et al., 2005). Several studies have suggested that hydrogel-based microfluidic fabrication techniques play an essential role in achieving a 3D cell culture environment for drug screening. In this case, branched, serpentine, spiral, and 3D interconnected structures can be constructed with the advantage of vascular function in pathological and physiological situations (Fig. 8b) (Nie et al., 2018). Moreover, Fig. 8c depicts the hydrogel-based complex helical microfibers and cell-laden helical microfibers, which can be designed into several geometries, including multilayer helical and superhelical hollow microfluidic structures with winding channels to mimic the structural characteristics and swirl blood flow in the blood vessels (Jia et al., 2019). These geometrical designs of microfluidic channels are potentially used to screen drugs for cardiovascular diseases such as atherosclerosis (Li et al., 2019).

Furthermore, bloodstream infections, such as sepsis, are life threatening worldwide (Hsieh and Huang, 2022). Their timely detection and treatment by applying antibiotics at a suitable concentration can

Table 2
Comparison for effect of different sensing materials on sensing properties of microfluidic sensors.

Type of sensing materials	Sensing materials	Target analyte	Linear range	LOD	Refs.
Carbon-based materials	rGO	Isoproterenol	1 nM–10 μM	–	Li et al. (2019)
	CDQs	Ketamine	200 μM–1000 μM	200 μM	Yehia et al. (2020)
	Graphene	Dopamine	0.5 μM–120 μM	0.01 μM	Manbohi and Ahmadi (2019)
Nanoparticle-based materials	AuNPs	Phenol	10 nM–200 nM	2.91 nM	Caetano et al. (2018)
	AuNPs	Methamphetamine	50 nM–0.1 μM	30 nM	Kline et al. (2016)
	AuNPs	Nicotine	12 μM–37 μM	11 μM	Adamo et al. (2020)
DNA and aptamer-based	dsDNA	BPA	43.8 nM–219 μM	43.8 nM	Liu et al. (2018)
Materials	Aptamer	Cocaine	14.5 fM – 14.5 pM	7.8 fM	Oueslati et al. (2018)

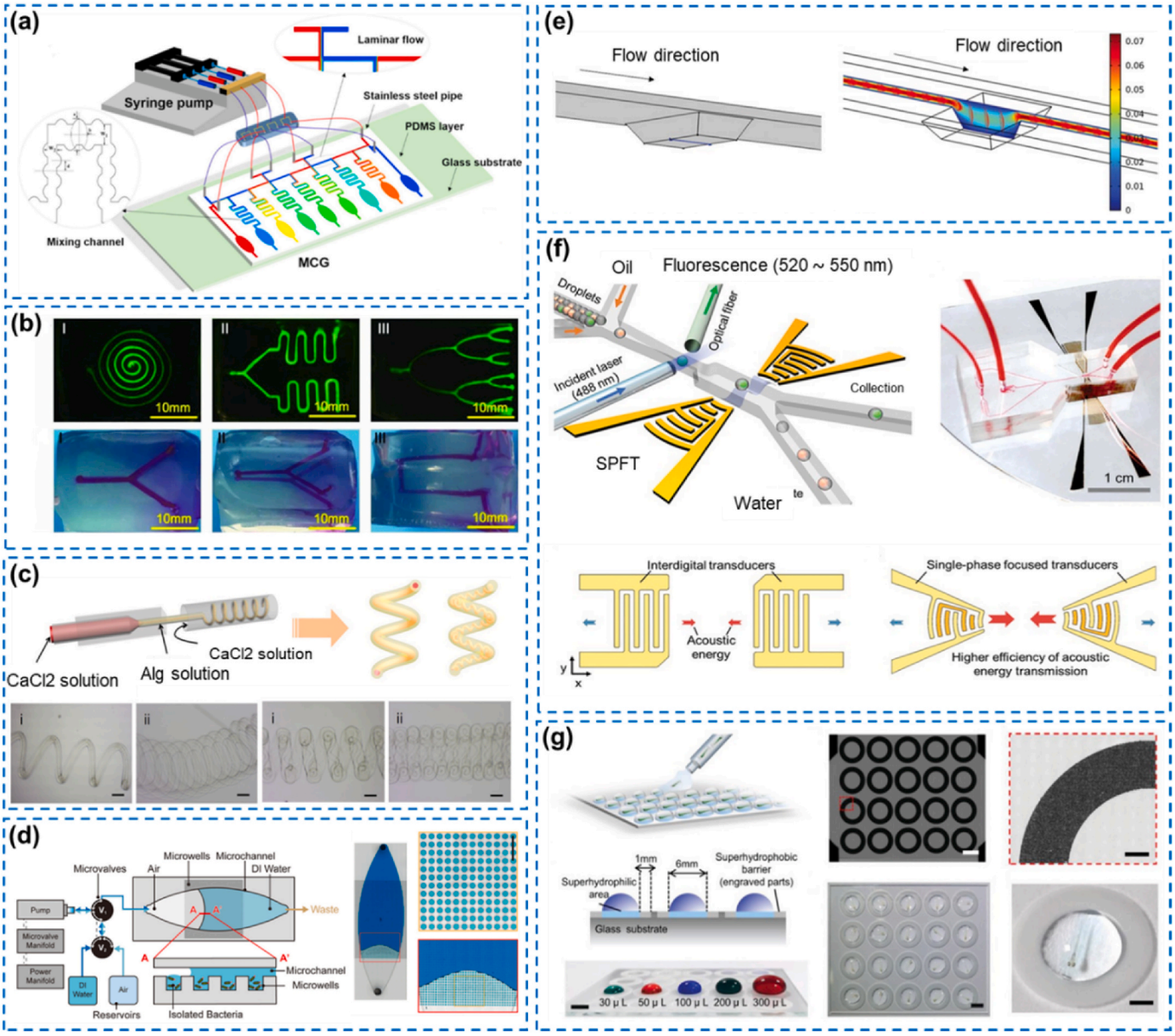

Fig. 8. Representative examples of diverse geometries of different microfluidic platforms. (a) A concentration gradient generator-based microfluidic device and a wide range of flow rates, reproduced with permission from (Shi et al., 2019), copyright 2019 Elsevier. (b) Schematic of branched, spiral, serpentine, and 3D-interconnected forms of microfluidic channels for developing vascularized tissue or organ models, reproduced with permission from (Nie et al., 2018), copyright 2018 Wiley-VCH. (c) Illustration of the hydrogel-based helical hollow microfibers to mimic the structural characteristics and swirl blood flow in the blood vessels, reproduced with permission from (Li et al., 2019), copyright 2019 Wiley-VCH. (d) An olive-shaped microfluidic microwell device to encounter the bobble generation in SERS-AST protocol, reproduced with permission from (Liao et al., 2021), copyright 2021 Elsevier. (e) A 3D advection-diffusion model of the microfluidic cavity using computational fluid dynamics (CFD), reproduced with permission from (Kohl et al., 2021), copyright 2021 Wiley-VCH. (f) Schematic of a single-phase focused transducer-based droplet sorter for biocompatible drug screening, reproduced with permission from (Zhong et al., 2021), copyright 2021 Wiley-VCH. (g) A fish capsule-based high-throughput drug screening system, reproduced with permission from (Tang et al., 2022), copyright 2022 Wiley-VCH.

determine the patient's survival. The olive-shaped microfluidic system depicted in Fig. 8d was proposed to simplify and standardize the conventional SERS-antimicrobial susceptibility testing (AST) protocol, which can perform rapid bacterial eradication with the aid of antibiotics. In the SERS-AST protocol, bubble generation during air isolation is a critical problem that can hamper the detection process. Herein, the olive-like geometry plays the most critical role in eliminating bobble generation (Liao et al., 2021). Hence, directly or indirectly, the geometry of the microfluidic system is one of the most critical factors in drug screening applications. Before fabricating the microfluidic platform, the structure of the microcavity and microchannel can be a computed to optimize its geometry because any undesirable flow will affect the transport of species to the cells and high-throughput drug screening. Fig. 8e shows the simulated flow of the fluids in the microfluidic system and the use of COMSOL Multiphysics to determine the system requirements for cellular and multiorgan level assessment and new drug screening (Kohl et al., 2021). Recent advances have also enabled the utilization of microfluidics-based platforms for single-droplet-based drug screening. The single-phase focused transducer (SPFT) droplet sorting device shows a great response in biocompatible drug screening at the droplet level. The SPFT sorter device depicted in Fig. 8f was used to screen the cytotoxicity of doxorubicin on cancer and noncancer cells. It can achieve a high throughput of over 1182 events per second, whereas the power consumption is less (16 Vpp), and the cell viability rate can be

maintained at 93.5% in the post shorting condition. Herein, the geometrical designs and dimensions of the single-phase focused transducer play a significant role in the high efficiency of acoustic energy transmission to achieve sorting purity up to 99.2%. Meanwhile, the acoustofluidics-based design ensures the unidirectional propagation of acoustic waves focused on the sorting region (Zhong et al., 2021). Meanwhile, multiorgan drug scanning can be achieved by a novel fish capsule microfluidic system, as shown in Fig. 8g, which combines microencapsulating technology with machine learning algorithms. This transparent geometrical structure enables multiorgan, multifunctional, high-throughput, large-scale screening with multiorgan imaging and functional analysis of specific organs. The other advantage of this system is combinational drug screening. It requires only limited amounts of samples and resources to accelerate the identification of novel therapeutics for precision medicines (Tang et al., 2022).

In addition, multiorgan microfluidic models have also been used to mimic a liver-on-a-chip to study drug metabolism, which is vital for detoxification and homeostasis in the human body. Herein, microphysiological systems (MPSs) have emerged as the most influential culture system for drug screening and disease modeling in liver-based microorgan models. In the 'PREDICT-96 platform', devised in 2019, the PREDICT-96 array is integrated with a micropumping system (PREDICT-96 pump) capable of recirculating medium at ultralow volumes. The unique geometry and low volume footprint of the platform in the MPS enable the observation of hepatitis response, including secretion feedback to any drug or stimuli. Thus, current limitations associated with drug screening via MSPs can be addressed by the PREDICT-96 platform (Tan et al., 2019). However, this kind of complex organ cultivation model under proper physiological conditions also faces challenges in maintaining its functions over time (Alépée et al., 2014).

4.2. Different morphologies on the surface of the microfluidic sensing platform

The manipulation of the surface of the microfluidic system with nano or microstructures can enhance the practical functions of the microfluidic systems. Nano/microstructures with different morphologies have been proposed for the modification of microchannels, which is crucial for improving the sensitivity of drug screening. Raman spectroscopy combined with the nanogap structure is predominantly utilized for level-free chemical sensing (Lin et al., 2017). Interestingly, in 2020, Lao et al. fabricated a SERS microfluidic device with a self-assembled metal nanogap structure. These nanogap plasmonic structures on the surface of microfluidic systems were designed using the switchable self-assembly method. In this study, nanopillars are fabricated by a laser printing method, and then the combined effect of supercritical drying and capillary-force driven self-assembly (CFSA) is utilized by the authors. The authors suggested that the as-formed nanogap morphologies enhanced the electromagnetic fields, which in turn improved the SERS signals by factors of up to $\approx 8 \times 10^7$ (Fig. 8a), thus facilitating localized and level-free sensing of anticancer drugs such as DOX (Lao et al., 2020). Furthermore, Dies et al. designed a unique dendritic architecture onto the SERS substrate for the screening of certain illicit drugs, such as oxycodone, cocaine, and heroin, in body fluids, such as saliva. These substrates are designed on a reusable microelectrode platform by electrokinetically gathering colloidal silver nanoparticles. The utilization of the dendritic nanostructures provided highly dense SERS hotspots to enhance the system's detection capability up to 100% accuracy for illicit drug screening (Dies et al., 2018). Thus, the inclusion of surface morphologies shows promising results in SERS-based detection modules for drug sensing and screening.

For approximately ten years, circulating tumor cell (CTC) detection technology has been recognized as one of the most promising tools for the diagnosis of cancer in the early stage (Poudineh et al., 2018). Various 3D micro/nanostructures are used to capture the CTC to observe the high-throughput drug screening on these cells and understand the cellular behavior upon drug injection in the microfluidic system. Fig. 8b shows a hierarchical spiky microstraw array (HS-MSA) integrated with a microfluidic device to demonstrate the dual functions of capturing cancer cells and the in situ chemical manipulations of those cells. The incorporation of these 3D micro/nanostructures of the HS-MSA enabled the capture of cancer cells with high efficiency (≈84%) and strong specificity. Thus, the 3D micro/nanostructure-based microfluidic system is not only a promising candidate for CTC detection but also promises new opportunities for the high-throughput screening of drugs against CTCs (He et al., 2019). To achieve high-throughput assays, the mechanical and chemical gradient generation ability of the microfluidic system is essential. Typically, the Christmas tree-like microfluidic structure is considered a standard structure for chemical gradient generation at the outlet (Wolfram et al., 2016). Fig. 9c depicts two designs of the gradient-generating microfluidic circuit combined with the microchambers, which enables cell culture as well as mechanical and chemical gradient generation on these cultured cells. In the first microchamber, there is no microstructure. However, in the second, micropillar structures are embedded in the chamber, which generates the gradient within the chamber. Thus, changing the microchamber morphology helps to achieve a chemical gradient within the chamber, which facilitates the effect of different drug concentrations and shear stresses. Furthermore, this design facilitates the coculture of different cell types at controlled ratios. In addition, the simulation results using COMSOL software show the local gradient generation of the micropillar-embedded chamber and plain chamber. Thus, the microfluidic channel morphology and structure enable the analysis of different flow rate conditions on the same device, which makes high-throughput drug screening more efficient (Jaberi et al., 2020). Moreover, the multiparametric screening of drugs is essential to reduce the financial burden, lengthy clinical trials, and high failure rate. The microfluidic multisized spheroid array can be an effective model to address these problems. This spheroid array can optimize cell culture conditions with different seeding densities and culture cell ratios. As shown in Fig. 9d, five different geometries of the microwell structures or different microfluidic channels were fabricated for developing blood–brain barrier (BBB) spheroids for multiparametric drug screening. The different shapes included spheres, flat-bottom wells, elliptic paraboloids, spherical caps, and hemispheres, which had specific effects on the drug penetration ability. The smaller BBB spheroids show 80% higher compound penetration capability than larger BBB spheroids. Hence, this microfluidic system's design and shape improve the potential drug screening outcomes (Eilenberger et al., 2021). Thus, the importance of surface morphology in microfluidic drug screening is discussed.

5. Applications of microfluidic drug sensing and screening

5.1. Therapeutic drug screening

Currently, the growth of the aging population and of antibiotic resistance are rapidly increasing to dangerous levels, and the recently produced therapeutic agents are becoming ineffectual exponentially faster than in previous years. Therefore, the screening and sensing of therapeutic drugs are greatly needed. Therapeutic drug screening, also known as therapeutic drug monitoring (TDM), is a drug therapy that can measure the concentration of drugs in blood, saliva, tears, sweat, urine, and ISF (Johnston and Holt, 1999; Kang and Lee, 2009; Raymundo-Pereira et al., 2022). Moreover, it assures accurate and precise dosage for each patient with minimal side effects for increased therapeutic efficiency. Currently, the commercials and traditional techniques used for drug monitoring suffer from issues such as high time consumption, high cost, and limited resources. In this regard, microfluidics-based biosensors for therapeutic drug sensing have emerged as a promising format for point-of-care testing.

Three-electrode systems in microfluidic chips play an important role in therapeutic drug sensing. However, most electrodes are planar with a

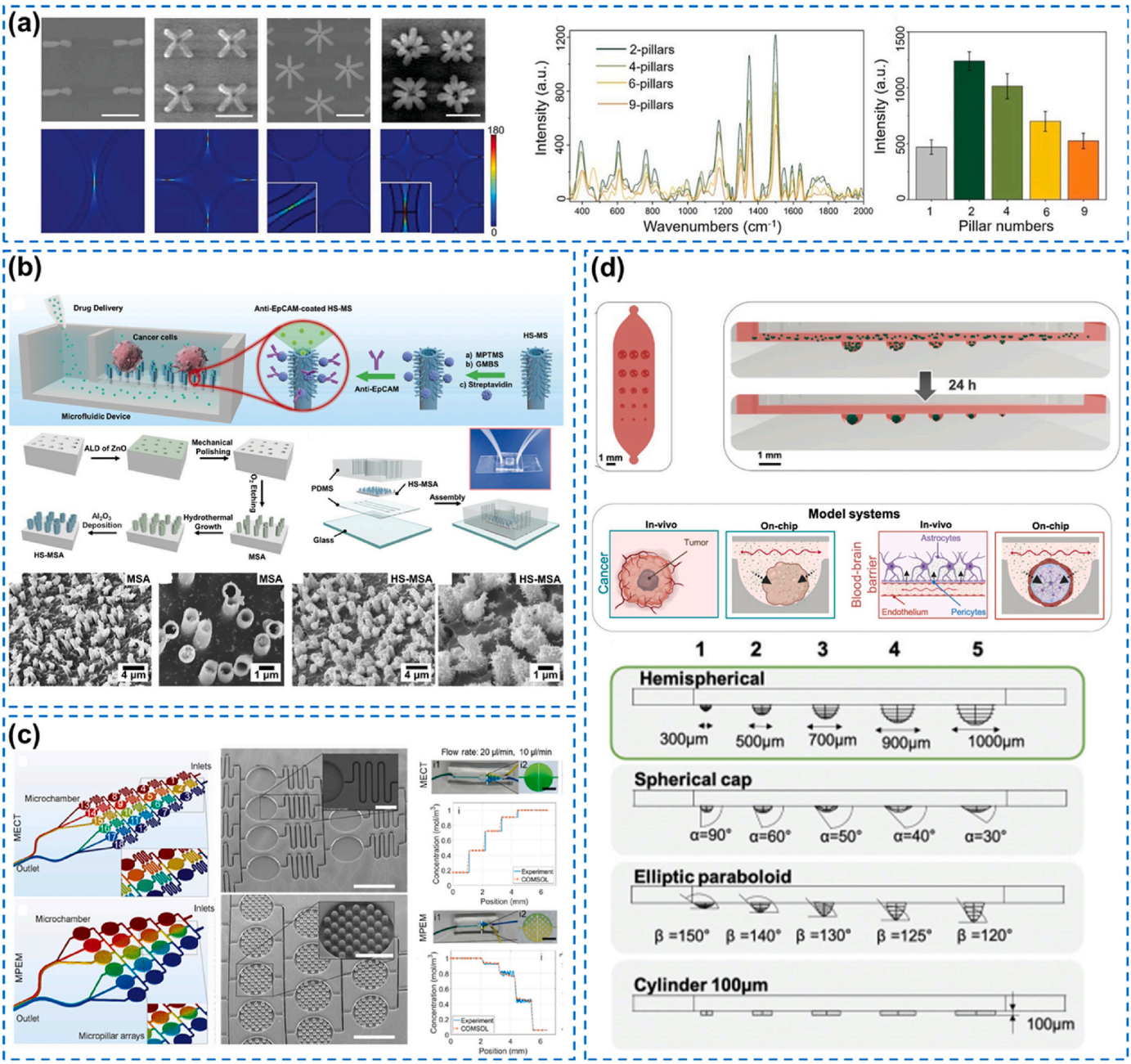

Fig. 9. Representative examples of different morphologies on the surface of microfluidic platforms. (a) A 3D nanogap plasmonic structure-embedded microfluidic device to enhance the SERS signal, reproduced with permission from (Lao et al., 2020), copyright 2020 Wiley-VCH. (b) A schematic illustration of the microfluidic device with hierarchical spiky microstraw structures captures CTCs, reproduced with permission from (He et al., 2019), copyright 2019 Wiley-VCH. (c) Designs of a micropillar-embedded microfluidic device for gradient generation within the microchamber, reproduced with permission from (Jaberi et al., 2020), copyright 2020 American Chemical Society. (d) A multisize and differently shaped microcavity array to control the spheroid size and growth dynamics, reproduced with permission from (Eilenberger et al., 2021), copyright 2021 Wiley-VCH.

limited effective area that generates only a nanoampere-level current signal (Chikkaveeraiah et al., 2011). Environmental factors can easily influence these signals and are unfavorable for highly sensitive sensing. Considering this issue, a simple and low-cost microfluidic device was fabricated for sensing three therapeutic drugs, warfarin sodium (WFS), cyclophosphamide, and carbamazepine, based on Pt wire as both a counter and a reference electrode and an Au–Ag alloy microwire (NPAMW) modified with 3D nanoporous and molecularly imprinted polymer as a working electrode. WFS was measured based on the gate effect with a linear response from 2×10^{-11} to 4×10^{-9} M with an LOD of 8×10^{-12} M, which can satisfy clinical assays (Fig. 10a) (Liu et al., 2017). For monitoring biological drugs such as adalimumab (ADM), for which true point-of-care (POC) testing remains lacking, an ADM biosensor has been developed for the first time by demonstrating the fiber optic surface plasmon resonance (FO-SPR) technique with a self-powered microfluidic device, which shows an LOD of 0.35 µg/mL. In comparison with existing POC biosensors for ADM quantification, this innovative biosensor requires only 1 µL of plasma, which is satisfactory. For the quantification of ADM, an in-house-developed FO-SPR platform was established with a short TTR for 20-fold diluted plasma, which shows comparable LOD to that of commercial FO-SPR (Fig. 10b) (Qu et al., 2022).

Following this, a novel "whole blood in-result out" self-powered microfluidic chip is demonstrated, which detects ADM within 30 min.

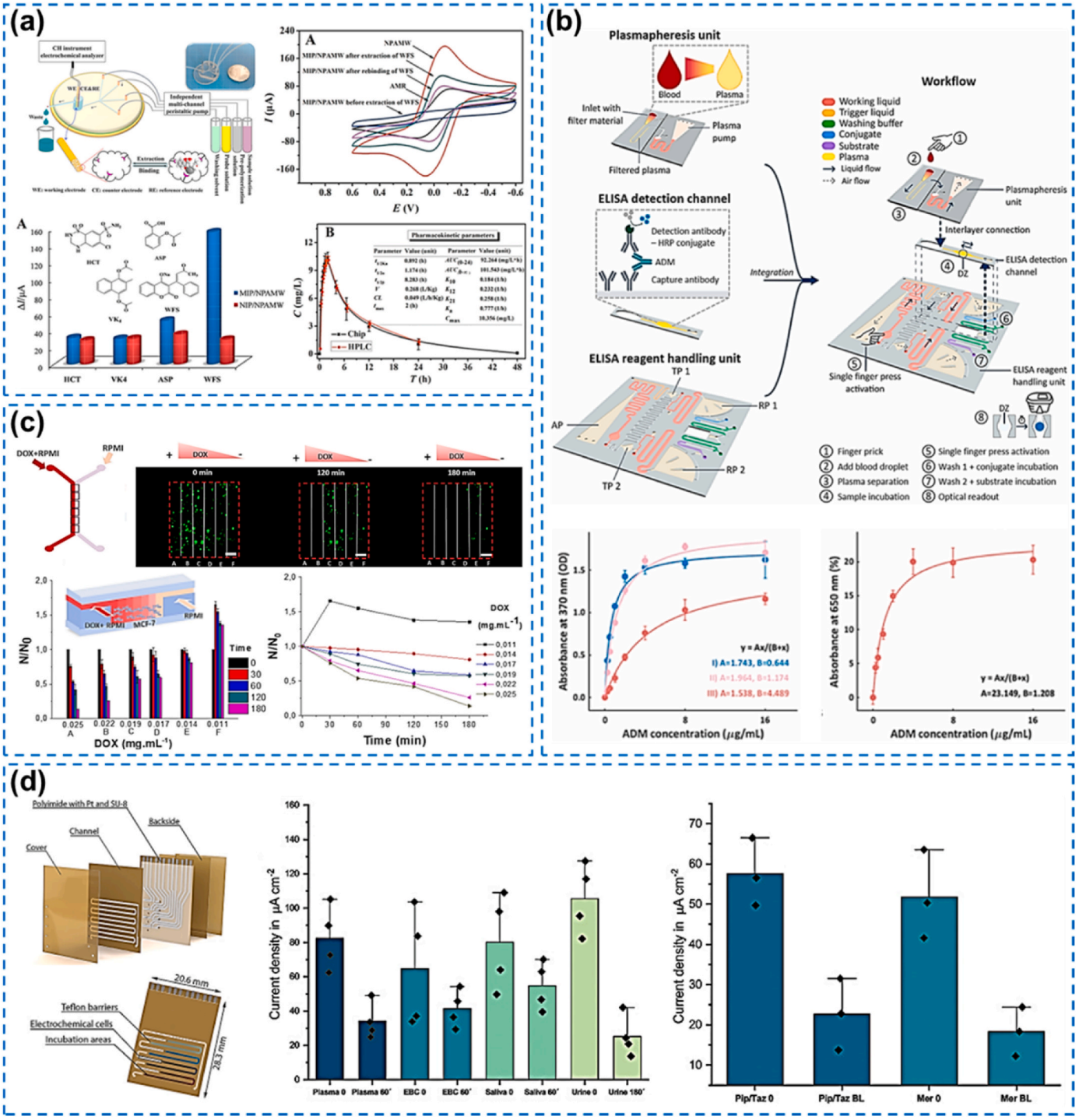

Fig. 10. Illustration of microfluidic devices for therapeutic drug sensing. (a) Illustration of the structure of the chip and sensing responses of the MIP/NIP-decorated NPAMR to WFS, reproduced with permission from (Liu et al., 2017), copyright 2017 Elsevier. (b) A 3D view of the cartridge design with the integrated FO probe and one-step FO-SPR bioassay for ADM detection, reproduced with permission from (Qu et al., 2022), copyright 2022 Elsevier. (c) Schematic depiction of self-powered ADM detection chip and all its components with ADM ELISA optimization, reproduced with permission from (Ordutowski et al., 2022), copyright 2022 Elsevier. (d) 3D rendering of the stacked multiplexed biosensor (Biosensor X) and time-dependent analysis of two different ß-lactams in plasma samples of animals given normal dosages of piperacillin/tazobactam and meropenem, reproduced with permission from (Ates et al., 2022), copyright 2022 Wiley-VCH.

This chip is activated by a single finger pressing and consists of two units, plasmapheresis for the rapid separation of plasma from whole blood within 5 min and an ELISA reagent handling unit, which detects ADM by an optimized POC-compatible sandwich ELISA protocol, where immobilization of capture antibody at the detection zone in the channel takes place. In Fig. 10c, sharp peaks of ADM in a concentration range of 0–16 μg/mL were obtained by shortening the sample conjugation and incubation time from 16 to 2 h to 2 min each. Moreover, to demonstration low-volume compatibility in POC conditions, an additional reduction from 100-200 μL to 25–50 μL showed an undisturbed signal. Hence, this chip provides a solution for therapeutic drug sensing of therapeutic antibodies at the patient's bedside or doctor's office (Ordutowski et al., 2022). On the other hand, breath can be used as a potential alternative candidate to bypass issues related to blood

transportation in microfluidic channels. Therefore, a versatile, disposable, and polymer-based microfluidic sensor was employed for the first time to sense piperacillin/tazobactam in exhaled breath condensate (EBC) to study the relation between plasma and EBC drug levels. Fig. 10d shows a proposed low-cost, rapid, sample-independent, and multiplexed onsite drug sensing device that can shift toward a "one-size-fits-all" strategy by tracking highly sensitive β-lactam concentrations in untreated blood samples of Landrace pigs treated with low, normal, and excessive dosages of piperacillin/tazobactam (Ates et al., 2022). Compared to a typical electrochemical sensor, which requires precautions such as a protective coating to minimize the deterioration caused by complex biofluids, the immobilization zone and electrochemical cell with a hydrophobic barrier are separated to bypass fouling issues, enabling the measurement of complex biofluids and the simultaneous measurement of different analytes on the same chip. Furthermore, therapeutic drug screening by microfluidics can be employed in health care units in the future for ease of use, miniature size, and its highly accurate selection of patient dosage in real time.

5.2. Illicit drug screening

In recent years, illicit drug abuse and addiction have become severe problems worldwide (Peacock et al., 2018). In addition to the growing number of new illicit drugs, the age group who use illicit drugs is also becoming younger yearly (Yin et al., 2019). Even a low dose of these drugs may result in physical and psychological damage and even death. Hence, illicit drug control has become an essential issue. To control the abuse of illicit drugs, detection and analysis methods are crucial (Mao et al., 2020; Musile et al., 2021; Noviana et al., 2020). The analysis of illicit drugs usually needs to overcome several problems. First, a low target analyte concentration must be detectible (Hilton et al., 2011; Jang et al., 2012; Kong et al., 2018; Paul et al., 2021). Second, the matrix present in real samples may influence the analysis and detection accuracy. It is necessary to have precise and accurate analytical measurements of the target drug in the complex background of real samples (Abdelshafi et al., 2019; Kim et al., 2020; Wägli et al., 2013; Zhang et al., 2014). Furthermore, the detection of illegal drugs sometimes requires immediate and accurate results. In this regard, microfluidics-based devices for drug sensing and screening show promising results.

The long-term and high-dose intake of methamphetamine (MA) may

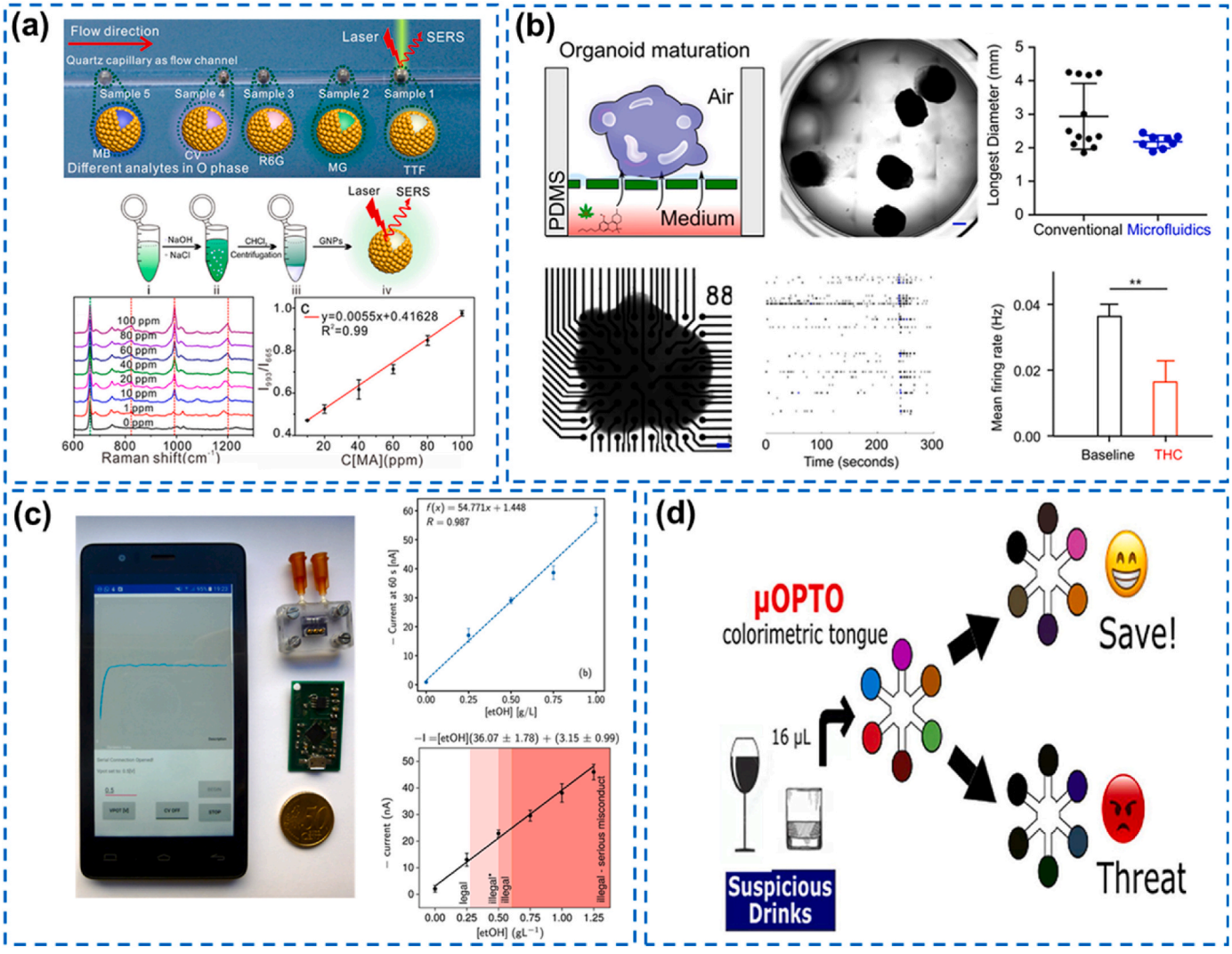

Fig. 11. Illustrations of the sensing and screening of different illicit drugs by microfluidic platforms. (a) An online mirrorlike PCM device to detect methamphetamine, reproduced with permission from (Su et al., 2019), copyright 2019 American Chemical Society. (b) Schematic of one-stop microfluidic brain organoid assembly to screen for the effect of cannabis exposure, reproduced with permission from (Ao et al., 2020), copyright 2020 American Chemical Society. (c) Schematic of a smartphone-based alcohol detection system in a whole blood sample, reproduced with permission from (Aymerich et al., 2018), copyright 2018 Elsevier. (d) A paper-based microfluidic tongue for alkaloid drug sensing and screening, reproduced with permission from (Dias et al., 2021), copyright 2021 Elsevier.

lead to psychotic symptoms, depression, anxiety, and fatigue. Considering this issue, Su et al., in 2019 devised a mirrorlike plasmonic capsule microfluidic (PCM) platform, as shown in Fig. 11a. This system combined citrate capped AuNP arrays with the SERS technique utilized to achieve efficient trace detection and quantitative measurement of MA. Moreover, the microfluidic device uses an oil/water (O/W) two-liquid interface to separate each analyte and a SERS system to detect MA in non-pretreated human saliva and urine (Su et al., 2019). In some cases, abusive drugs kill human brain cells. In that case, a culture medium of human cerebral organoids can provide a means to study the effect of these illicit drugs (e.g., cannabis). Accordingly, a one-stop microfluidic platform to culture human embryonic stem cells was developed by Ao and coworkers. This system can deliver quantitative analyses of the effects of the psychoactive cannabinoid Δ-9-tetrahydrocannabinol (THC) on targets from stem cells to a single organoid (Fig. 11b) (Ao et al., 2020). Alcohol concentration detection in whole-blood samples and saliva can be essential in law enforcement and medical emergencies. Therefore, Aymerich et al. developed a smartphone-based microfluidic system with potentiostatic amperometric measurement to measure alcohol concentration with a linear response in the range of 0–1.25 g L^{-1} and high sensitivity of 54 nA/g L^{-1}. Furthermore, a novel readout technique was used for the on-site, rapid, and cost-effective determination of the alcohol in blood on a standard Android smartphone (Fig. 11c) (Aymerich et al., 2018). In a similar vein, Dias et al. fabricated a paper-based microfluidic optoelectronic tongue to screen and sense eight different alkaloid drugs (i.e., atropine, scopolamine, morphine, cocaine, ephedrine, dipyrone, caffeine, and alprazolam). In this system, six well-known μOPTO (microfluidic paper-based optoelectronic)-based indicators were utilized to perform rapid on-scene identification via chemical reaction, which results in a color change. The six circular spots and the interconnected sample injection circle of the analytical microfluidic device were fabricated by employing the wax printing method (Fig. 11d) (Dias et al., 2021).

6. Conclusions and future perspectives

Recent global pandemics and acceleration in human health issues in the past few decades have indicated a great need for the early-stage detection of diseases, screening for bioanalytes and drug metabolites and drug abuse is also in high demand to provide continuous health monitoring. Hence, a comprehensive review highlighting the recent advances in microfluidic drug sensing and screening has been proposed. In this review, important factors such as sensing techniques, sensing and fabrication materials, the morphology and structure of microfluidic channels, and applications of drug sensing have been explored in detail. Till now, many of the microfluidic devices have been commercialized by many of the companies like, Roche Diagnostics, Dolomite, Droplet Genomics, PreciGenome, Agilent Technologies, i-STAT corp. (Abbott Laboratories), etc. based on integration of microfluidic chips with electrochemical and optical detection techniques. These commercialized devices are being used in POC diagnosis, cell analysis, food safety, drug analysis and delivery, and biomarker analysis. Nevertheless, there are still many multidisciplinary and tremendous endeavors in both science and engineering to accelerate the development of microfluidic devices. However, there are still some challenges in microfluidic devices like, creation of valves in hard substrates like glass and silicon, large number of steps in fabrication and operation, high level lab safety requirements, etc. Moreover, drug screening with microfluidic devices still faces some challenges, such as the interaction of nonspecific molecules with the sensing surface and the complete integration of the drug analysis system as a single device. However, few researchers have employed alternative currents to prevent the influence of the matrix, which is an approach that can be used in future work to resolve the influence of nonspecific molecules. In addition, some researchers have developed thread-based microfluidic devices for drug screening that can be good candidates for rapid and low-cost screening in the future. After reviewing the factors involved in microfluidic drug sensing mentioned above, it can be concluded that there are many drugs for which microfluidic sensing platforms can be developed using specific properties of materials, such as the optical properties of DNA, as well as metal nanoparticles (AuNPs, AgNPs) and organoids on chips.

Author statement

Arnab Pal and Kuldeep Kaswan worked on conceptualization, methodology, and writing. Snigdha Roy Barman and Manish Kumar Sharma worked on the writing and discussion of the manuscript. Yu-Zih Lin, Jun-Hsuan Chung, Kuei-Lin Liu, Bo-Huan Chen, and Chih-Cheng Wu worked on writing and editing. Sangmin Lee, Dongwhi Choi, and Zong-Hong Lin worked on conceptualization and supervision for this manuscript. Zong-Hong Lin took the lead in writing the manuscript, providing critical feedback, and helping to shape the manuscript.

Declaration of competing interest

The authors declare that they have no known competing financial interests or personal relationships that could have appeared to influence the work reported in this paper.

Data availability

No data was used for the research described in the article.

Acknowledgments

This work was financially supported from the Young Scholar Fellowship Program by the Ministry of Science and Technology of Taiwan (111-2636-E-007-022), the National Tsing Hua University Research Grant, and the Chung-Ang University Research Grant in 2022.

References

Abdelshafi, N.A., Bell, J., Rurack, K., Schneider, R.J., 2019. Drug Test. Anal. 11 (3), 492–500.
Adamo, C.B., Junger, A.S., Bressan, L.P., da Silva, J.A.F., Poppi, R.J., de Jesus, D.P., 2020. Microchem. J. 156, 104985.
Ahi, E.E., Torul, H., Zengin, A., Sucularlı, F., Yıldırım, E., Selbes, Y., Suludere, Z., Tamer, U., 2022. Biosens. Bioelectron. 195, 113660.
Ahmed, T., Shimizu, T.S., Stocker, R., 2010. Nano Lett. 10 (9), 3379–3385.
Ai, X., Wu, Y., Lu, W., Zhang, X., Zhao, L., Tu, P., Wang, K.W., Jiang, Y., 2020. Adv. Sci. 7 (11), 2000111.
Alépée, N., Bahinski, A., Daneshian, M., de Wever, B., Fritsche, E., Goldberg, A., Hansmann, J., Hartung, T., Haycock, J., Hogberg, H.T., Hoelting, L., Kelm, J.M., Kadereit, S., Mcvey, E., Landsiedel, R., Leist, M., Lübberstedt, M., Noor, F., Pellevoisin, C., Zurich, M.-G., 2014. ALTEX 31 (4), 441–477.
Andreou, C., Hoonejani, M.R., Barmi, M.R., Moskovits, M., Meinhart, C.D., 2013. ACS Nano 7 (8), 7157–7164.
Ansari, N., Lodha, A., Pandya, A., Menon, S.K., 2017. Anal. Methods 9 (38), 5632–5639.
Ansari, M.I.H., Hassan, S., Qurashi, A., Khanday, F.A., 2016. Biosens. Bioelectron. 85, 247–260.
Ao, Z., Cai, H., Havert, D.J., Wu, Z., Gong, Z., Beggs, J.M., Mackie, K., Guo, F., 2020. Anal. Chem. 92 (6), 4630–4638.
Ates, H.C., Mohsenin, H., Wenzel, C., Glatz, R.T., Wagner, H.J., Bruch, R., Hoefflin, N., Spassov, S., Streicher, L., Lozano-Zahonero, S., Flamm, B., Trittler, R., Hug, M.J., Köhn, M., Schmidt, J., Schumann, S., Urban, G.A., Weber, W., Dincer, C., 2022. Adv. Mater. 34 (2), 2104555.
Aymerich, J., Márquez, A., Terés, L., Muñoz-Berbel, X., Jiménez, C., Domínguez, C., Serra-Graells, F., Dei, M., 2018. Biosens. Bioelectron. 117, 736–742.
Baker, M.J., Trevisan, J., Bassan, P., Bhargava, R., Butler, H.J., Dorling, K.M., Fielden, P. R., Fogarty, S.W., Fullwood, N.J., Heys, K.A., Hughes, C., Lasch, P., Martin-Hirsch, P. L., Obinaju, B., Sockalingum, G.D., Sulé-Suso, J., Strong, R.J., Walsh, M.J., Wood, B. R., Gardner, P., Martin, F.L., 2014. Nat. Protoc. 9 (8), 1771–1791.
Bandaru, P., Chu, D., Sun, W., Lasli, S., Zhao, C., Hou, S., Zhang, S., Ni, J., Cefaloni, G., Ahadian, S., Dokmeci, M.R., Sengupta, S., Lee, J., Khademhosseini, A., 2019. Small 15 (15), 1900300.
Bavli, D., Prill, S., Ezra, E., Levy, G., Cohen, M., Vinken, M., Vanfleteren, J., Jaeger, M., Nahmias, Y., 2016. Proc. Natl. Acad. Sci. USA 113 (16), 2231–2240.
Berthier, E., Beebe, D.J., 2014. Lab Chip 14 (17), 3241–3247.
Caetano, F.R., Carneiro, E.A., Agustini, D., Figueiredo-Filho, L.C.S., Banks, C.E., Bergamini, M.F., Marcolino-Junior, L.H., 2018. Biosens. Bioelectron. 99, 382–388.

Cao, X., Ashfaq, R., Cheng, F., Maharjan, S., Li, J., Ying, G., Hassan, S., Xiao, H., Yue, K., Zhang, Y.S., 2019. Adv. Funct. Mater. 29 (31), 1807173.
Carroll, D., Morzaria, S., Briand, S., Johnson, C.K., Morens, D., Sumption, K., Tomori, O., Wacharphaueasadee, S., 2021. BMJ Br. Med. J. 372, n485.
Chawla, K., Modena, M.M., Ravaynia, P.S., Lombardo, F.C., Leonhardt, M., Panic, G., Bürgel, S.C., Keiser, J., Hierlemann, A., 2018. ACS Sens. 3 (12), 2613–2620.
Chatterjee, S., Saha, S., Barman, S.R., Khan, I., Pao, Y.P., Lee, S., Choi, D., Lin, Z.H., 2020. Nano Energy 77, 105093.
Chen, H.J., Miller, P., Shuler, M.L., 2018. Lab Chip 18 (14), 2036–2046.
Chowdhury, M.S., Zheng, W., Kumari, S., Heyman, J., Zhang, X., Dey, P., Weitz, D.A., Haag, R., 2019. Nat. Commun. 10 (1), 4546.
Chen, T., Yin, S., Wu, J., 2021. TrAC - Trends Anal. Chem. 142, 116309.
Chen, X., Zhang, S., Han, W., Wu, Z., Chen, Y., Wang, S., 2018. J. Chem. Technol. Biotechnol. 93 (12), 3353–3363.
Chikkaveeraiah, B.v., Mani, V., Patel, V., Gutkind, J.S., Rusling, J.F., 2011. Biosens. Bioelectron. 26 (11), 4477–4483.
Choi, J.H., Lee, J., Oh, B.K., 2016. Biochip J. 10, 331–345.
Choi, N.W., Cabodi, M., Held, B., Gleghorn, J.P., Bonassar, L.J., Stroock, A.D., 2007. Nat. Mater. 6 (11), 908–915.
Das, J., Cederquist, K.B., Zaragoza, A.A., Lee, P.E., Sargent, E.H., Kelley, S.O., 2012. Nat. Chem. 4, 642–648.
Delalat, B., Cozzi, C., Rasi Ghaemi, S., Polito, G., Kriel, F.H., Michl, T.D., Harding, F.J., Priest, C., Barillaro, G., Voelcker, N.H., 2018. Adv. Funct. Mater. 28 (28), 1801825.
Derda, R., Tang, S., Laromaine, A., Mosadegh, B., Hong, E., Mwangi, M., Mammoto, A., Ingber, D., Whitesides, G., 2011. PLoS One 6 (5), e18940.
Dhiman, N., Kingshott, P., Sumer, H., Sharma, C.S., Rath, S.N., 2019. Biosens. Bioelectron. 137, 236–254.
Dias, B.C., Batista, A.D., da Silveira Petruci, J.F., 2021. Anal. Chim. Acta 1187, 339141.
Dies, H., Raveendran, J., Escobedo, C., Docoslis, A., 2018. Sens. Actuators B Chem. 257, 382–388.
Domon, B., Aebersold, R., 2006. Science 312 (5771), 212–217.
Driouich, J.S., Cochin, M., Lingas, G., Moureau, G., Touret, F., Petit, P.R., Piorkowski, G., Barthélémy, K., Laprie, C., Coutard, B., Guedj, J., de Lamballerie, X., Solas, C., Nougairède, A., 2021. Nat. Commun. 12 (1), 1735.
Dutse, S.W., Yusof, N.A., 2011. Sensors 11 (6), 5754–5768.
Eduati, F., Utharala, R., Madhavan, D., Neumann, U.P., Longerich, T., Cramer, T., Saez-Rodriguez, J., Merten, C.A., 2018. Nat. Commun. 9 (1), 2434.
Eilenberger, C., Rothbauer, M., Selinger, F., Gerhartl, A., Jordan, C., Harasek, M., Schädl, B., Grillari, J., Weghuber, J., Neuhaus, W., Küpcü, S., Ertl, P., 2021. Adv. Sci. 8 (11), 2004856.
Feng, Q., Liu, J., Li, X., Chen, Q., Sun, J., Shi, X., Ding, B., Yu, H., Li, Y., Jiang, X., 2017. Small 13 (9), 1603109.
Fu, S. xia, Zuo, P., Ye, B.C., 2021. Biotechnol. J. 16 (2), 2000126.
Gérard, A., Woolfe, A., Mottet, G., Reichen, M., Castrillon, C., Menrath, V., Ellouze, S., Poitou, A., Doineau, R., Briseno-Roa, L., Canales-Herrerias, P., Mary, P., Rose, G., Ortega, C., Delincé, M., Essono, S., Jia, B., Iannascoli, B., Richard-Le Goff, O., Brenan, C., 2020. Nat. Biotechnol. 38 (6), 715–721.
Gasper, R., Dewelle, J., Kiss, R., Mijatovic, T., Goormaghtigh, E., 2009. Biochim. Biophys. Acta Biomembr. 1788 (6), 1263–1270.
Harrer, S., Shah, P., Antony, B., Hu, J., 2019. Trends Pharmacol. Sci. 40 (8), 577–591.
He, G., Yang, C., Feng, J., Wu, J., Zhou, L., Wen, R., Huang, S., Wu, Q., Liu, F., Chen, H.J., Hang, T., Xie, X., 2019. Adv. Funct. Mater. 29 (12), 1806484.
Hilton, J.P., Nguyen, T.H., Pei, R., Stojanovic, M., Lin, Q., 2011. Sens. Actuator A Phys. 166 (2), 241–246.
Hsieh, C.Y., Huang, N.T., 2022. Sens. Actuators B Chem. 359, 131580.
Hu, Z., Chen, X., Wang, L., 2018. Chem. Eng. Technol. 41 (3), 489–495.
Hu, X., Hu, X., Zhao, S., Zhao, S., Luo, Z., Zuo, Y., Zuo, Y., Wang, F., Wang, F., Zhu, J., Zhu, J., Chen, L., Chen, L., Yang, D., Zheng, Yajing, Zheng, Yujia, Cheng, Y., Zhou, F., Yang, Y., Yang, Y., 2020. Lab Chip 20 (12), 2228–2236.
Huang, X., Jain, P.K., El-Sayed, I.H., El-Sayed, M.A., 2007. Nanomedicine 2 (5), 681–693.
Humphries, R.M., Ferraro, M.J., Hindler, J.A., 2018. J. Clin. Microbiol. 56 (5), e00139, 18.
Ilacas, G.C., Basa, A., Nelms, K.J., Sosa, J.D., Liu, Y., Gomez, F.A., 2019. Anal. Chim. Acta 1055, 74–80.
Jaberi, A., Monemian Esfahani, A., Aghabaglou, F., Park, J.S., Ndao, S., Tamayol, A., Yang, R., 2020. ACS Appl. Bio Mater. 3 (10), 6661–6671.
Jain, R.K., Au, P., Tam, J., Duda, D.G., Fukumura, D., 2005. Nat. Biotechnol. 23, 821–823.
Jang, E., Kim, S., Koh, W.G., 2012. Biosens. Bioelectron. 31 (1), 529–536.
Jeon, N.L., Dertinger, S.K.W., Chiu, D.T., Choi, I.S., Stroock, A.D., Whitesides, G.M., 2000. Langmuir 16 (22), 8311–8316.
Jia, L., Han, F., Yang, H., Turnbull, G., Wang, J., Clarke, J., Shu, W., Guo, M., Li, B., 2019. Adv. Healthc. Mater. 8 (13), 1900435.
Jiang, X., Ng, J.M.K., Stroock, A.D., Dertinger, S.K.W., Whitesides, G.M., 2003. J. Am. Chem. Soc. 125 (18), 5294–5295.
Jin, Y., Kim, J., Lee, J.S., Min, S., Kim, S., Ahn, D.H., Kim, Y.G., Cho, S.W., 2018. Adv. Funct. Mater. 28 (37), 1801954.
Johnston, A., Holt, D.W., 1999. Br. J. Clin. Pharmacol. 47 (4), 339–350.
Jung, D.J., Shin, T.H., Kim, M., Sung, C.O., Jang, S.J., Jeong, G.S., 2019. Lab Chip 19 (17), 2854–2865.
Kang, J.S., Lee, M.H., 2009. Korean J. Intern. Med. 24 (1), 1–10.
Kazoe, Y., Shimizu, Y., Morikawa, K., Terui, Y., Irie, T., Kitamori, T., 2021. Sens. Actuators B Chem. 340, 129957.
Kim, S.B., Koo, J., Yoon, J., Hourlier-Fargette, A., Lee, B., Chen, S., Jo, S., Choi, J., Oh, Y. S., Lee, G., Won, S.M., Aranyosi, A.J., Lee, S.P., Model, J.B., Braun, P.V., Ghaffari, R., Park, C., Rogers, J.A., 2020. Lab Chip 20 (1), 84–92.
Kim, S.S., Kim, Y.R., Chung, T.D., Sohn, B.H., 2014. Adv. Funct. Mater. 24 (19), 2738-2738.
Kline, N.D., Tripathi, A., Mirsafavi, R., Pardoe, I., Moskovits, M., Meinhart, C., Guicheteau, J.A., Christesen, S.D., Fountain, A.W., 2016. Anal. Chem. 88 (21), 10513–10522.
Koh, E.H., Lee, W.C., Choi, Y.J., Moon, J. il, Jang, J., Park, S.G., Choo, J., Kim, D.H., Jung, H.S., 2021. ACS Appl. Mater. Interfaces 13 (2), 3024–3032.
Kohl, Y., Biehl, M., Spring, S., Hesler, M., Ogourtsov, V., Todorovic, M., Owen, J., Elje, E., Kopecka, K., Moriones, O.H., Bastús, N.G., Simon, P., Dubaj, T., Rundén-Pran, E., Puntes, V., William, N., von Briesen, H., Wagner, S., Kapur, N., Knoll, T., 2021. Small 17 (15), 2006012.
Kong, X., Chong, X., Squire, K., Wang, A.X., 2018. Sens. Actuators B Chem. 259, 587–595.
Korzhenko, O., Führer, P., Göldner, V., Olthuis, W., Odijk, M., Karst, U., 2021. Anal. Chem. 93 (37), 12740–12747.
Kratz, C., Furchner, A., Oates, T.W.H., Janasek, D., Hinrichs, K., 2018. ACS Sens. 3 (2), 299–303.
Lao, Z., Zheng, Y., Dai, Y., Hu, Y., Ni, J., Ji, S., Cai, Z., Smith, Z.J., Li, J., Zhang, L., Wu, D., Chu, J., 2020. Adv. Funct. Mater. 30 (15), 1909467.
Laschke, M.W., Harder, Y., Amon, M., Martin, I., Farhadi, J., Ring, A., Torio-Padron, N., Schramm, R., Rücker, M., Rücker, R., Junker, D., Jö, J., Häufel, J.M., Häufel, H., Carvalho, C., Heberer, M., Gü, G., Germann, G., Vollmar, B., Menger, M.D., 2006. Tissue Eng. 12 (8), 2093–2104.
Lee, W. bin, Chien, C.C., You, H.L., Kuo, F.C., Lee, M.S., Lee, G. bin, 2019b. Lab Chip 19 (16), 2699–2708.
Lee, H., Hong, Y.J., Baik, S., Hyeon, T., Kim, D.H., 2018. Adv. Healthc. Mater. 7 (8), 1701150.
Lee, J., Kim, S.E., Moon, D., Doh, J., 2021. Lab Chip 21 (11), 2142–2152.
Lee, J.B., Park, J.S., Shin, Y.M., Lee, D.H., Yoon, J.K., Kim, D.H., Ko, U.H., Kim, Y.T., Bae, S.H., Sung, H.J., 2019a. Adv. Funct. Mater. 29 (23), 1900075.
Li, H., Garner, T., Diaz, F., Wong, P.K., 2019. Small 15 (28), 1901910.
Li, L., Chen, Z., Shao, C., Sun, Lingyu, Sun, Lingyun, Zhao, Y., 2020. Adv. Funct. Mater. 30 (3), 1906353.
Li, Y., Shi, G., Du, J., Wang, J., Bian, P., 2019. Biomech. Model. Mechanobiol. 18 (2), 411–423.
Li, Zhenghui, Li, Zhaopeng, Li, L., Li, C., Zhong, W., Zhang, H., 2017. ACS Appl. Mater. Interfaces 9 (18), 15557–15565.
Liang, Y., Cui, W., Li, L., Yu, Z., Peng, W., Xu, T., 2019. Adv. Opt. Mater. 7 (7), 1970026.
Liao, C.C., Chen, Y.Z., Lin, S.J., Cheng, H.W., Wang, J.K., Wang, Y.L., Han, Y.Y., Huang, N.T., 2021. Biosens. Bioelectron. 191, 113483.
Lin, D., Wu, Z., Li, S., Zhao, W., Ma, C., Wang, J., Jiang, Z., Zhong, Z., Zheng, Y., Yang, X., 2017. ACS Nano 11 (2), 1478–1487.
Lin, D., Li, P., Feng, J., Lin, Z., Chen, X., Yang, N., Wang, L., Liu, D., 2020. Small 16 (9), 1901001.
Lin, N., Zhou, X., Geng, X., Drewell, C., Hübner, J., Li, Z., Zhang, Y., Xue, M., Marx, U., Li, B., 2020. Sci. Rep. 10 (1), 8879.
Lin, X., Sun, X., Luo, S., Liu, B., Yang, C., 2016. TrAC - Trends Anal. Chem. 80, 132–148.
Liu, C.C., Wang, Y.N., Fu, L.M., Huang, Y.H., 2018. Chem. Eng. J. 332, 695–701.
Liu, H., Bolonduro, O.A., Hu, N., Ju, J., Rao, A.A., Duffy, B.M., Huang, Z., Black, L.D., Timko, B.P., 2020. Nano Lett. 20 (4), 2585–2593.
Liu, J., Zhang, Y., Jiang, M., Tian, L., Sun, S., Zhao, N., Zhao, F., Li, Y., 2017. Biosens. Bioelectron. 91, 714–720.
Liu, S., Fu, Y., Xiong, C., Liu, Z., Zheng, L., Yan, F., 2018. ACS Appl. Mater. Interfaces 10 (28), 23522–23528.
Liu, W., Sun, M., Lu, B., Yan, M., Han, K., Wang, J., 2019. Sens. Actuators B Chem. 292, 111–120.
Liu, W., Lin, J.M., 2016. ACS Sens. 1 (4), 344–347.
Liu, X., Zheng, W., Jiang, X., 2019. ACS Sens. 4 (6), 1465–1475.
Liu, Y., Sun, L., Zhang, H., Shang, L., Zhao, Y., 2021. Chem. Rev. 121 (13), 7468–7529.
Liu, Y., Wei, X., Chen, J., Yu, Y.-L., Wang, J.-H., Qiu, H., 2022. Anal. Chem. 94 (15), 5970–5979.
Looby, N.T., Tascon, M., Acquaro, V.R., Reyes-Garcés, N., Vasiljevic, T., Gomez-Rios, G. A., Wasowicz, M., Pawliszyn, J., 2019. Analyst 144 (12), 3721–3728.
Ma, K., Xie, W., Liu, W., Wang, L., Wang, D., Tang, B.Z., 2021. Adv. Funct. Mater. 31 (36), 2102645.
Manbohi, A., Ahmadi, S.H., 2019. Sens. Bio-Sens. Res. 23, 100270.
Materón, E.M., Lima, R.S., Joshi, N., Shimizu, F.M., Oliveira, O.N., 2018. Graphene-Based Electrochemical Sensors for Biomolecules: Micro and Nano Technologies, pp. 321–336.
Mao, K., Zhang, H., Pan, Y., Zhang, K., Cao, H., Li, X., Yang, Z., 2020. TrAC - Trends Anal. Chem. 130, 115975.
Mitchell, K.R., Esene, J.E., Woolley, A.T., 2022. Anal. Bioanal. Chem. 414, 167–180.
Mitxelena-Iribarren, O., Zabalo, J., Arana, S., Mujika, M., 2019. Biosens. Bioelectron. 123, 237–243.
Mullard, A., 2018. Nat. Rev. Drug Discov. 17 (10), 691–692.
Musile, G., Agard, Y., Wang, L., de Palo, E.F., McCord, B., Tagliaro, F., 2021. Trends Analyt. Chem. 143, 116406.
Muñoz, J., Montes, R., Baeza, M., 2017. TrAC - Trends Anal. Chem. 97, 201–215.
Naresh, V., Lee, N., 2021. Sensors 21 (4), 1109.
Nie, J., Gao, Q., Wang, Y., Zeng, J., Zhao, H., Sun, Y., Shen, J., Ramezani, H., Fu, Z., Liu, Z., Xiang, M., Fu, J., Zhao, P., Chen, W., He, Y., 2018. Small 14 (45), 1802368.
Noviana, E., Carrão, D.B., Pratiwi, R., Henry, C.S., 2020. Anal. Chim. Acta 1116, 70–90.

Nummelin, S., Kommeri, J., Kostiainen, M.A., Linko, V., 2018. Adv. Mater. 30 (24), 1870175.
Ordutowski, H., Dal Dosso, F., de Wispelaere, W., van Tricht, C., Vermeire, S., Geukens, N., Gils, A., Spasic, D., Lammertyn, J., 2022. Biosens. Bioelectron. 208, 114189.
Oueslati, R., Cheng, C., Wu, J., Chen, J., 2018. Biosens. Bioelectron. 108, 103–108.
Paek, J., Park, S.E., Lu, Q., Park, K.T., Cho, M., Oh, J.M., Kwon, K.W., Yi, Y.S., Song, J.W., Edelstein, H.I., Ishibashi, J., Yang, W., Myerson, J.W., Kiseleva, R.Y., Aprelev, P., Hood, E.D., Stambolian, D., Seale, P., Muzykantov, V.R., Huh, D., 2019. ACS Nano 13 (7), 7627–7643.
Pal, A., Chatterjee, S., Saha, S., Barman, S.R., Choi, D., Lee, S., Lin, Z.-H., 2020. ECS J. Solid State Sci. Technol. 9 (11), 115029.
Pao, Y.P., Yu, C.C., Lin, Y.Z., Chatterjee, S., Saha, S., Tiwari, N., Huang, Y.T., Wu, C.C., Choi, D., Lin, Z.H., 2021. Nano Energy 85, 106008.
Paul, M., Tannenberg, R., Tscheuschner, G., Ponader, M., Weller, M.G., 2021. Biosensors 11 (9), 12489.
Peacock, A., Leung, J., Larney, S., Colledge, S., Hickman, M., Rehm, J., Giovino, G.A., West, R., Hall, W., Griffiths, P., Ali, R., Gowing, L., Marsden, J., Ferrari, A.J., Grebely, J., Farrell, M., Degenhardt, L., 2018. Addiction 113 (10), 1905–1926.
Pei, H., Wan, Y., Li, J., Hu, H., Su, Y., Huang, Q., Fan, C., 2011. Chem. Commun. 47, 6254–6256.
Pejcic, B., DeMarco, R., 2006. Electrochim. Acta 51 (28), 6217–6229.
Pison, U., Welte, T., Giersig, M., Groneberg, D.A., 2006. Euro. J. Pharma. 533 (1–3), 341–350.
Poudineh, M., Sargent, E.H., Pantel, K., Kelley, S.O., 2018. Nat. Biomed. Eng. 2, 72–84.
Qian, Z., Fei, J., Zong, S., Yang, K., Li, L., Liu, R., Wang, Z., Cui, Y., 2020. ACS Sens. 5 (1), 208–216.
Qu, J.H., Ordutowski, H., van Tricht, C., Verbruggen, R., Barcenas Gallardo, A., Bulcaen, M., Ciwinska, M., Gutierrez Cisneros, C., Devriese, C., Guluzade, S., Janssens, X., Kornblum, S., Lu, Y., Marolt, N., Nanjappan, C., Rutten, E., Vanhauwaert, E., Geukens, N., Thomas, D., Dal Dosso, F., Safdar, S., Spasic, D., Lammertyn, J., 2022. Biosens. Bioelectron. 206, 114125.
Ramezankhani, R., Solhi, R., Chai, Y.C., Vosough, M., Verfaillie, C., 2022. Drug Discov. Today 27 (4), 1062–1076.
Raymundo-Pereira, P.A., Gomes, N.O., Machado, S.A.S., Oliveira, O.N., 2022. Chem. Eng. J. 435 (2), 135047.
Regnault, C., Dheeman, D.S., Hochstetter, A., 2018. High-Throughput 7 (2), 18.
Ren, K., Zhou, J., Wu, H., 2013. Acc. Chem. Res. 46 (11), 2396–2406.
Ren, L., Zhou, X., Nasiri, R., Fang, J., Jiang, X., Wang, C., Qu, M., Ling, H., Chen, Y., Xue, Y., Hartel, M.C., Tebon, P., Zhang, S., Kim, H.J., Yuan, X., Shamloo, A., Dokmeci, M.R., Li, S., Khademhosseini, A., Sun, W., 2020. Small Methods 4 (10), 202000438.
Rezvani Jalal, N., Mehrbod, P., Shojaei, S., Labouta, H.I., Mokarram, P., Afkhami, A., Madrakian, T., Los, M.J., Schaafsma, D., Giersig, M., Ahmadi, M., Ghavami, S., 2021. ACS Appl. Nano Mater. 4 (5), 4307–4328.
Robinson, N.B., Krieger, K., Khan, F., Huffman, W., Chang, M., Naik, A., Yongle, R., Hameed, I., Krieger, K., Girardi, L.N., Gaudino, M., 2019. Int. J. Surg. 72, 9–13.
Sabhachandani, P., Motwani, V., Cohen, N., Sarkar, S., Torchilin, V., Konry, T., 2016. Lab Chip 16 (3), 497–505.
Sadik, O.A., Aluoch, A.O., Zhou, A., 2009. Biosens. Bioelectron. 24 (9), 2749–2765.
Sanvicens, N., Marco, M.P., 2008. Trends Biotechnol. 26 (8), 425–433.
Sansa, M., Defoort, M., Brenac, A., Hermouet, M., Banniard, L., Fafin, A., Gely, M., Masselon, C., Favero, I., Jourdan, G., Hentz, S., 2020. Nat. Commun. 11 (1), 3781.
Shen, Y., Yi, J., Song, M., Li, D., Wu, Y., Liu, Y.J., Yang, M., Qiao, L., 2021. Analyst 146 (13), 4146–4153.
Sengupta, J., Hussain, C.M., 2019. TrAC - Trends Anal. Chem. 114, 326–337.
Schuster, B., Junkin, M., Kashaf, S.S., Romero-Calvo, I., Kirby, K., Matthews, J., Weber, C.R., Rzhetsky, A., White, K.P., Tay, S., 2020. Nat. Commun. 11, 5271.
Segawa, H., Fukuoka, T., Itoh, T., Imai, Y., Iwata, Y.T., Yamamuro, T., Kuwayama, K., Tsujikawa, K., Kanamori, T., Inoue, H., 2019. Analyst 144 (6), 2158–2165.
Senel, M., Dervisevic, E., Alhassen, S., Dervisevic, M., Alachkar, A., Cadarso, V.J., Voelcker, N.H., 2020. Anal. Chem. 92 (18), 12347–12355.
Shi, H., Hou, Z., Zhao, Y., Nie, K., Dong, B., Chao, L., Shang, S., Long, M., Liu, Z., 2019. Chem. Eng. J. 359, 1327–1338.
Shi, Y., Cai, Y., Cao, Y., Hong, Z., Chai, Y., 2021. TrAC - Trends Anal. Chem. 134, 116118.
Shin, S.R., Kilic, T., Zhang, Y.S., Avci, H., Hu, N., Kim, D., Branco, C., Aleman, J., Massa, S., Silvestri, A., Kang, J., Desalvo, A., Hussaini, M.A., Chae, S.K., Polini, A., Bhise, N., Hussain, M.A., Lee, H.Y., Dokmeci, M.R., Khademhosseini, A., 2017. Adv. Sci. 4 (5), 1600522.
Singh, S.U., Chatterjee, S., Lone, S.A., Ho, H.-H., Kaswan, K., Peringeth, K., Khan, A., Chiang, Y.-W., Lee, S., Lin, Z.-H., 2022. Microchim. Acta 189, 236.
Silvestrini, M., Fruk, L., Moretto, L.M., Ugo, P., 2015. J. Nanosci. Nanotechnol. 15 (5), 3437–3442.
Sivashanmugan, K., Squire, K., Tan, A., Zhao, Y., Kraai, J.A., Rorrer, G.L., Wang, A.X., 2019. ACS Sens. 4 (4), 1109–1117.
Skardal, A., Shupe, T., Atala, A., 2016. Drug Discov. Today 21 (9), 1399–1411.
Soldano, C., Mahmood, A., Dujardin, E., 2010. Carbon 48 (8), 2127–2150.
Song, D., Jung, Y., 2019. Angew. Chem. Int. Ed. 58 (7), 2045–2049.
Song, Y., Lee, S., Ko, Y., Huh, J., Kim, Y., Yeom, B., Moon, J.H., Cho, J., 2022. Adv. Funct. Mater. 32 (2), 2270008.
Spencer, C.E., Rumbelow, S., Mellor, S., Duckett, C.J., Clench, M.R., 2022. Pharmaceutics 14 (2), 14020364.
Su, M., Jiang, Y., Yu, F., Yu, T., Du, S., Xu, Y., Yang, L., Liu, H., 2019. ACS Appl. Bio Mater. 2 (9), 3828–3835.
Sun, W.H., Wei, Y., Guo, X.L., Wu, Q., Di, X., Fang, Q., 2020. Anal. Chem. 92 (13), 8759–8767.
Telenti, A., Arvin, A., Corey, L., Corti, D., Diamond, M.S., García-Sastre, A., Garry, R.F., Holmes, Pang P.S., Virgin, H.W., 2021. Nature 596, 495–504.
Tan, K., Keegan, P., Rogers, M., Lu, M., Gosset, J.R., Charest, J., Bale, S.S., 2019. Lab Chip 19 (9), 1556–1566.
Tang, M., Duan, X., Yang, A., He, S., Zhou, Y., Liu, Y., Zhang, L., Luo, X., Shi, P., Li, H., Lin, X., 2022. Adv. Sci. 9 (9), 202104449.
Tang, Q., Li, X., Lai, C., Li, L., Wu, H., Wang, Y., Shi, X., 2021. Bioact. Mater. 6 (1), 169–178.
Tascon, M., Alam, M.N., Gómez-Ríos, G.A., Pawliszyn, J., 2018. Anal. Chem. 90 (4), 2631–2638.
Teymourian, H., Parrilla, M., Sempionatto, J.R., Montiel, N.F., Barfidokht, A., VanEchelpoel, R., DeWael, K., Wang, J., 2020. ACS Sens. 5 (9), 2679–2700.
Tiwari, N., Chatterjee, S., Kaswan, K., Chung, J.H., Fan, K.P., Lin, Z.H., 2022. J. Electroanal. Chem. 907, 116064.
Theobald, J., Ghanem, A., Wallisch, P., Banaeiyan, A.A., Andrade-Navarro, M.A., Taškova, K., Haltmeier, M., Kurtz, A., Becker, H., Reuter, S., Mrowka, R., Cheng, X., Wölfl, S., 2018. ACS Biomater. Sci. Eng. 4 (1), 78–89.
Tung, N.T., Tue, P.T., Thi Ngoc Lien, T., Ohno, Y., Maehashi, K., Matsumoto, K., Nishigaki, K., Biyani, M., Takamura, Y., 2017. Sci. Rep. 7, 17881.
Valencia, P.M., Farokhzad, O.C., Karnik, R., Langer, R., 2012. Nat. Nanotechnol. 7 (10), 623–629.
Walther, B.K., Dinu, C.Z., Guldi, D.M., Sergeyev, V.G., Creager, S.E., Cooke, J.P., Guiseppi-Elie, A., 2020. Mater. Today 39, 23–46.
Wang, L., Wu, J.T., 2018. Nat. Commun. 9, 218.
Wang, Y.I., Carmona, C., Hickman, J.J., Shuler, M.L., 2018. Adv. Healthcare Mater. 7 (2), 1701000.
Wägli, P., Chang, Y.C., Homsy, A., Hvozdara, L., Herzig, H.P., de Rooij, N.F., 2013. Anal. Chem. 85 (15), 7558–7565.
Wang, Y., Hu, A., 2014. J. Mater. Chem. C 2 (34), 6921–6939.
Wee, Y., Park, S., Kwon, Y.H., Ju, Y., Yeon, K.M., Kim, J., 2019. Biosens. Bioelectron. 132, 279–285.
Weltin, A., Slotwinski, K., Kieninger, J., Moser, I., Jobst, G., Wego, M., Ehret, R., Urban, G.A., 2014. Lab Chip 14 (1), 138–146.
Wolfram, C.J., Rubloff, G.W., Luo, X., 2016. Biomicrofluidics 10 (6), 061301.
Wu, J., Jie, M., Dong, X., Qi, H., Lin, J.M., 2016. Rapid Commun. Mass Spectrom. 30 (S1), 80–86.
Wu, L., Xiong, E., Zhang, Xia, Zhang, Xiaohua, Chen, J., 2014. Nano Today 9 (2), 197–211.
Wu, D., Qin, M., Xu, D., Wang, L., Liu, C., Ren, J., Zhou, G., Chen, C., Yang, F., Li, Y., Zhao, Y., Huang, R., Pourtaheri, S., Kang, C., Kamata, M., Chen, I.S.Y., He, Z., Wen, J., Chen, W., Lu, Y., 2019. Adv. Mater. 31 (18), 1970127.
Xie, X., Zhang, W., Abbaspourrad, A., Ahn, J., Bader, A., Bose, S., Vegas, A., Lin, J., Tao, J., Hang, T., Lee, H., Iverson, N., Bisker, G., Li, L., Strano, M.S., Weitz, D.A., Anderson, D.G., 2017. Nano Lett. 17 (3), 2015–2020.
Xu, Z., Gao, Y., Hao, Y., Li, E., Wang, Y., Zhang, J., Wang, W., Gao, Z., Wang, Q., 2013. Biomaterials 34 (16), 4109–4117.
Xu, K., Fujita, Y., Lu, Y., Honda, S., Shiomi, M., Arie, T., Akita, S., Takei, K., 2021. Adv. Mater. 33 (18), 2170141.
Yakob, L., 2022. Emerg. Infect. Dis. 28 (4), 837–840.
Yang, L., Kim, T.H., Cho, H.Y., Luo, J., Lee, J.M., Chueng, S.T.D., Hou, Y., Yin, P.T.T., Han, J., Kim, J.H., Chung, B.G., Choi, J.W., Lee, K.B., 2021. Adv. Funct. Mater. 31 (5), 2006918.
Yehia, A.M., Farag, M.A., Tantawy, M.A., 2020. Anal. Chim. Acta 1104, 95–104.
Yezhelyev, M. v, Gao, X., Xing, Y., Al-Hajj, A., Nie, S., O'regan, R.M., 2006. Lancet Oncol. 7 (8), 657–667.
Yin, S., M. P, H., 2019. Clin. Pediatr. Emerg. Med. 20 (1), 17–24.
Yu, Y., Nyein, H.Y.Y., Gao, W., Javey, A., 2020. Adv. Mater. 32 (15), 2070115.
Yue, S., Fang, J., Xu, Z., 2022. Biosens. Bioelectron. 198, 113822.
Zhai, J., Yi, S., Jia, Y., Mak, P.I., Martins, R.P., 2019. TrAC - Trends Anal. Chem. 117, 231–241.
Zhang, F., Qu, K.Y., Zhou, B., Luo, Y., Zhu, Z., Pan, D.J., Cui, C., Zhu, Y., Chen, M.L., Huang, N.P., 2021. Biosens. Bioelectron. 179, 113080.
Zhang, H., Hu, X., Fu, X., 2014. Biosens. Bioelectron. 57, 22–29.
Zhang, D., Zhang, Y., Yin, F., Qin, Q., Bi, H., Liu, B., Qiao, L., 2021. Analyst 146 (2), 515–520.
Zhao, Q., Cui, H., Wang, Y., Du, X., 2020. Small 16 (9), 1903798.
Zhao, S.K., Hu, X.J., Zhu, J.M., Luo, Z.Y., Liang, L., Yang, D.Y., Chen, Y.L., Chen, L.F., Zheng, Y.J., Hu, Q.H., Zheng, J.J., Guo, S.S., Cheng, Y.X., Zhou, F.L., Yang, Y., 2021. Lab Chip 21 (20), 4005–4015.
Zhao, Y., Tang, M., Liu, F., Li, H., Wang, H., Xu, D., 2019. Anal. Chem. 19 (21), 13418–13426.
Zheng, Y., Wu, Z., Lin, J.M., Lin, L., 2020. Chin. Chem. Lett. 31 (2), 451–454.
Zheng, F., Fu, F., Cheng, Y., Wang, C., Zhao, Y., Gu, Z., 2016. Small 12 (17), 2253–2282.
Zheng, L., Wang, B., Sun, Y., Dai, B., Fu, Y., Zhang, Y., Wang, Y., Yang, Z., Sun, Z., Zhuang, S., Zhang, D., 2021. ACS Sens. 6 (3), 823–832.
Zhong, R., Yang, S., Ugolini, G.S., Naquin, T., Zhang, J., Yang, K., Xia, J., Konry, T., Huang, T.J., 2021. Small 17 (46), 2103848.
Zhu, L., Liu, X., Yang, J., He, Y., Li, Y., 2020. Anal. Chem. 92 (17), 11981–11986.
Zhu, Y., Sun, L., Wang, Y., Cai, L., Zhang, Z., Shang, Y., Zhao, Y., 2022. Adv. Mater. 34 (13), 202108972.